

**EPIDEMIOLOGICAL CRITERIA AND DEEP CONVOLUTIONAL
NEURAL NETWORKS FOR EFFICIENT SELECTION OF CULTIVARS
AGAINST THE WHEAT BLAST DISEASE**

by

Mariela Sofia Fernández Campos

A Thesis

Submitted to the Faculty of Purdue University

In Partial Fulfillment of the Requirements for the degree of

Master of Science



Department of Botany and Plant Pathology

West Lafayette, Indiana

December 2020

**THE PURDUE UNIVERSITY GRADUATE SCHOOL
STATEMENT OF COMMITTEE APPROVAL**

Dr. Christian D. Cruz, Chair

Department of Botany and Plant Pathology

Dr. Darcy E. P. Telenko

Department of Botany and Plant Pathology

Dr. Mohammad R. Jahanshahi

Lyles School of Civil Engineering

Dr. Robert L. Nielsen

Department of Agronomy

Approved by:

Dr. Christopher Staiger

Dedicated to God, my mom, family, mentors (angels), and friends who always have been there believing, supporting, and encouraging me. I also want to dedicate it to all the Ticas, Latinas, and Zamoranas who have big dreams and work intentionally every day to accomplish them. To Brenson, for his support during the Covid-19 pandemic and last year of my master's program.

ACKNOWLEDGMENTS

I want to thank Dr. C. D. Cruz for allowing me to be part of his hard-working team, his mentoring, life lessons, encouragement, and sharing his knowledge. A special thanks to Dr. Gongora for the late nights of temporal and spatial analysis, tons of statistics, writing, and philosophical discussions. You are a true friend! Andres Cruz, thanks for your help, motivation, and for being a great team member!

I would also like to thank Dr. Mohammad Jahanshahi, Yu-Ting Huang, and Tao Wang for their mentoring and help with the development of the deep convolutional neural network model. Special thanks to Dr. Darcy Telenko and Dr. Robert Nielsen for their questions, comments, and suggestions. I am so grateful for having learned so much from you.

Without the hard work of our Bolivian team, these studies would not have been possible. Thanks to Ing. MSc. Diego Baldelomar, Ing. MSc. Gabriela Rivadeneira, Ing. Lidia Calderón, Ing. Jorge Cuellar, Ing. Darwin Coimbra, Ing. Franklin Cortez, and other collaborators.

I want to thank my colleagues Paula Zapata, Joel Mercado, Katherine Rivera, Denise Cadwell, Ana Morales, Diana Salguero, the Association of Zamorano Alumni, and the Costa Rica Student Association at Purdue for their friendship, encouragement, and support during these years.

Thanks to Ligia Matousek, Dr. Carlos Rojas, Dr. Luis Gomez, M. Eng. Monica Sorribas, Dr. Christopher Voglewede, Dr. Courtney Gallup, and MBA. Alejandro Cedeño who paved the way to work as an intern at Dow AgroSciences (Indianapolis and Costa Rica) and contributed to my learning. That inspiring experience opened my vision and allowed me to learn and interact with many great scientists and leaders. I want to acknowledge my former supervisors, MSc. Todd Mathieson, Dr. Marc Fishers, and Dr. Bob Masters, the Biological Characterization Researcher Team and Fungicide Discovery team for their mentoring and advice. I will be eternally grateful!

TABLE OF CONTENTS

LIST OF TABLES	7
LIST OF FIGURES	9
ABSTRACT	10
CHAPTER 1. INTRODUCTION	11
1.1 References	13
CHAPTER 2. EPIDEMIOLOGICAL CRITERIA TO SUPPORT BREEDING TACTICS AGAINST THE EMERGING, HIGH CONSEQUENCE WHEAT BLAST DISEASE	17
2.1 Introduction.....	17
2.2 Materials and methods	18
2.2.1 Locations.....	18
2.2.2 Genetic materials and crop management.....	18
2.2.3 Experimental design	19
2.2.4 Visual disease assessment and grain weight.....	20
2.2.5 Data analysis	20
2.3 Results.....	21
2.3.1 Temporal modeling.....	25
2.3.2 Effect of cultivar resistance on disease and grain weight.....	31
2.3.3 Correlation among disease parameters	37
2.4 Discussion.....	39
2.5 References.....	43
CHAPTER 3. WHEAT SPIKE BLAST IMAGE CLASSIFICATION USING DEEP CONVOLUTIONAL NEURAL NETWORKS.....	47
3.1 Introduction.....	47
3.2 Materials and methods	49
3.2.1 Plant cultivation and genetic materials	49
3.2.2 Inoculation	50
3.2.3 Data collection	50
3.2.4 Disease severity	51
3.2.5 Inter-rater agreement of wheat spike blast severity estimations.....	51

3.2.6	Data.....	53
3.2.7	Deep learning model.....	56
3.2.8	Model performance evaluation	58
3.3	Results.....	59
3.3.1	Cultivar response to wheat spike blast under controlled conditions.....	59
3.3.2	Inter-rater agreement analysis.....	59
3.3.3	Deep convolutional neural networks model performance.....	61
3.4	Discussion.....	66
3.5	Conclusion	67
3.6	References.....	68

LIST OF TABLES

Table 2.1 List of cultivars of different wheat spike blast resistance groups planted in two locations in Bolivia during the 2018-2019 season.	19
Table 2.2. Analysis of variance of repeated measurement analysis of wheat blast severity ($Pr > F$) in different plant organs in Bermejo, Bolivia, during the 2018-2019 season.	22
Table 2.3. Analysis of variance of repeated measurement analysis of wheat blast severity ($Pr > F$) in different plant organs in Quirusillas, Bolivia, during the 2018-2019 season.	23
Table 2.4. Parameters of the pairwise comparison T-test of three susceptible cultivars for wheat blast severity in two experiments with different spreader design at two locations in Bolivia, 2018-2019.....	24
Table 2.5. Summary of statistical parameters of four linearized temporal growth models for wheat blast severity in two locations in Bolivia 2018-2019.....	27
Table 2.6. Summary of statistical parameters and Akaike's information criterium (AIC) and delta Akaike's information criterium (Δ AIC) of linearized logistic and Gompertz models for ten cultivars at two locations in Bolivia in 2018-2019.	29
Table 2.7. Main effect of resistance (among ten cultivars) on wheat blast severity at two locations in Bolivia in 2018-2019.	35
Table 2.8. Pearson correlation coefficients for total area under the disease progress curve (tAUDPC), linearized logistic infection rate of disease progress (r_L^*), final wheat blast disease severity (Y_{max}), grain weight, in two locations in Bolivia, 2018-2019.....	38
Table 3.1. Final wheat spike blast severity (Y_{max}) of wheat cultivars assessed at 19 days after inoculation.....	50
Table 3.2. Severity ranges of wheat spike blast images per category.....	51
Table 3.3. Training and testing data distribution and number of images in Dataset 1 (maturing and non-matured spikes).....	56
Table 3.4. Training and testing data distribution and number of images in Dataset 2 (non-matured spikes only).....	56
Table 3.5. Two datasets trained the four cases of study with different loss functions in three categories. [Category 1: 0%, Category 2: 0.1-20%, Category 3: 20.1-100% severity]	58
Table 3.6. Values of accuracy ₁ (ρ_c), precision ₁ (r), and bias (Cb) for agreement between raters' visual estimations and disease measurements of ImageJ in both datasets of wheat spike blast...	60
Table 3.7. Values of weighted Kappa (κ) analysis for inter-rater agreement between raters and ImageJ in two datasets of wheat spike blast under controlled environment.....	61
Table 3.8. Values of Fleiss Kappa ($F\kappa$) analysis among two raters and ImageJ agreement in two datasets of wheat spike blast under a controlled environment.....	61

Table 3.9. Precision, recall and F_1 score of the test data for different model in both datasets. ... 63

LIST OF FIGURES

Figure 2.1. Disease progress curves for ten wheat cultivars (untransformed data y vs t (DAE: days after emergence)), in epidemics induced by *Magnaphorthe oryzae* pathotype *Triticum*. Disease progress curves show the wheat leaf blast and wheat spike blast severity across all plant organs (from leaf F-6 to spike). Experiments 1 (A) and 2 (B) at Bermejo, (C) and (D) at Quirusillas conducted during the 2018-2019 growing season. 25

Figure 2.2. The total area under the disease progress curve of wheat leaf and spike (tAUDPC) blast of ten wheat cultivars in location one (A) according to experiments one and two. Results for location two (B) include experiment one and experiment two. Experiments were conducted in Bolivia during the 2018-2019 wheat growing season..... 33

Figure 2.3. Area under the disease progress curve of wheat leaf and spike (AUDPC) blast of ten wheat cultivars in location one according to experiments one (A) and two (B). Results for location two include experiment one (C) and experiment two (D). Experiments were conducted in Bolivia during the 2018-2019 wheat growing season. 34

Figure 2.4. Linear regression between grain weight and wheat blast severity of ten cultivars, (A) and (B) experiments in location one (Bermejo), (C), and (D) experiments in location two (Quirusillas). Experiments were conducted in Bolivia during the 2018-2019 wheat growing season. 39

Figure 3.1. Flow process: (a) *Magnaphorthe oryzae* pathotype *Triticum* inoculation, (b) dew chamber provided optimal conditions for fungal infection, and (c) wheat spike imaging 50

Figure 3.2. Examples of images per category: (a-d) healthy wheat spikes no disease (0% severity, Category 1); (e-h) spikes with moderate severity (0.1-20 %, Category 2); and (i-l) spikes with high severity (20.1-100 %, Category 3). 55

Figure 3.3. Confusion matrix of the images of Dataset 1 (maturing and non-matured spikes): (A) Case 1, (B) Case 2, (C) Case 3 and (D) Case 4 65

Figure 3.4. Confusion matrix of the images of Dataset 1 (non-matured spikes only): (A) Case 1, (B) Case 2, (C) Case 3 and (D) Case 4 65

ABSTRACT

Wheat blast, a disease caused by the fungal pathogen *Magnaporthe oryzae pathotype Triticum*, threatens global wheat production. Limited epidemiological information makes the wheat blast disease hard to contain and control, and without data, recommendations about the selection and deployment of resistant cultivars remain a challenge. Besides, cultivar selection relies on human visual disease evaluations, which can be time-consuming, labor-intensive, and subjective. We hypothesized that epidemiological parameters could be relevant to support wheat blast breeding tactics, and reliable visual estimates paired with images of wheat spike blast could be used to train deep convolutional neural networks (DCNN) models for disease severity classification. To test these hypotheses, we focused on the following objectives: 1) to evaluate ten cultivars for wheat blast resistance under field conditions using epidemiological parameters, and 2) develop accurate and reliable DCNN models to classify wheat spike blast severity under controlled conditions. For objective 1, we evaluated wheat leaf blast and wheat spike blast severity and estimated the total area under the disease progress curve (tAUDPC), final disease severity, and epidemic type. Disease progress curves of ten cultivars were fitted by the logistic ($R^2=0.70-0.96$) and Gompertz ($R^2=0.64-0.94$) models, pointing out to polycyclic epidemics. We concluded that tAUDPC, disease progression rate, and final disease severity could support cultivar selection for wheat blast resistance. For objective 2, wheat spike blast severity was visually estimated, and Red Green Blue images were acquired from six cultivars with various resistance levels under controlled conditions. Severity estimations were paired with each wheat spike image and created two datasets. Dataset 1 (n=5,123) included maturing and non-matured wheat spikes, and Dataset 2 (n=4,509) had only non-matured spikes. Each dataset was analyzed for inter-rater agreement between disease severity estimation of two pathologists and disease measurements of Image J, then classified by severity categories to train and test the DCNN model. The model trained with only non-matured spikes had higher precision (0.90-0.95), F-1 (0.87-0.95), and recall (0.84-0.96) than the model trained with maturing and non-matured spikes (0.75-0.95, 0.79-0.95, and 0.74-0.96, respectively). We concluded that the trained DCNN model could be used as the basis of a phenotyping tool for wheat spike blast severity classification.

CHAPTER 1. INTRODUCTION

An emergent disease called wheat blast is a threat to the production of wheat (*Triticum aestivum*), the second-largest food crop for human consumption (FAOSTAT, 2017). Wheat blast is a disease caused by the *Ascomycetous* fungus, *Magnaphorthe oryzae* pathotype *Triticum* (MoT). This fungus was first detected in Brazil in 1985 and later dispersed to neighboring countries, including Bolivia, Paraguay, and Argentina (Barea and Toledo, 1996; Cabrera and Gutierrez, 2007; Igarashi et al., 1986; Parello et al., 2015; Viedma, 2005). Since then, an increasing intercontinental movement of MoT has occurred. In 2016, a wheat blast outbreak was first reported in Bangladesh (Malaker et al., 2016; Aman, 2016), apparently due to the unintentional importation of MoT-infected South American grain. Many countries in South Asia are actively monitoring wheat fields for the presence of MoT (Bhattacharya and Pal, 2017; Mottaleb et al., 2018). In 2020, the presence of MoT was reported in Zambia, Africa, which adds another continent to the list (Tembo et al., 2020). The wheat blast fungus is also a threat to wheat production in the U.S. (Cruz et al., 2016a). Risk analyses have predicted that if the pathogen is introduced and established in the U.S., it can affect soft and hard-red winter wheat production in several states (Cruz et al., 2016a).

Although MoT can infect leaves, stems, and seeds, the most described and studied symptoms are associated with spike blast. The spike encloses the grain, which is the plant's most valuable product (Cruz and Valent, 2017; Cruz et al., 2015; Igarashi et al., 1986). Wheat spike blast occurs when the fungus infects the spike, spikelets, or raquis (Igarashi, 1990). The infection can then cause bleached spikes, becoming visible and easy to differentiate from healthy heads. MoT can decrease grain quality and yield, and a wide range of disease intensity can occur depending on the cultivars planted and the prevalent weather conditions during the growing season (Goulart and Paiva, 1992).

The conducive conditions that lead to wheat blast outbreaks include a combination of warm temperatures, excessive rain, long and frequent spike wetness, use of susceptible cultivars, and poor fungicide efficacy (Goulart et al., 2007). The optimum conditions for wheat blast development include a temperature range between 25 to 30°C and spike surface wetness between 25 to 40 hours (based on controlled conditions) (Cardoso et al., 2008).

To protect wheat production from this emergent disease, there is a need for an increased understanding of the epidemiology of MoT. Plant disease epidemiology studies the increase in

disease intensity over time and space (Madden et al., 2007). Unfortunately, there are still many gaps in the epidemiological knowledge of wheat blast. Thus far, there are indications that wheat blast behaves as a polycyclic disease (Gongora-Canul et al., 2019). Therefore, after the occurrence of primary infections, which result from the contact between primary inoculum and host plants, secondary infections can occur during disease-conducive environmental conditions (Cruppe et al., 2019; Gomes et al., 2019; Gongora et al., 2019; Mills et al., 2020; Salgado et al., unpublished). Secondary infections result from inoculum produced during a current epidemic, and they occur only in polycyclic epidemics (Madden et al., 2007). For instance, there is evidence of the occurrence of wheat leaf blast infections and the vertical movement of symptoms up to the spike (Cruppe, 2019; Salgado et al., unpublished). Still, the occurrence and intensity of wheat spike and leaf blast in cultivars with different levels of reaction to the disease are not entirely understood. We hypothesize that increasing the wheat blast epidemiological knowledge can assist breeders during the cultivar selection process. For example, the disease rate of development can help predict how slow or fast the disease progresses. The area under the disease progress curve can help compare the reaction of cultivars to disease. Ultimately, final disease severity will determine the highest disease severity that may occur on a cultivar.

Currently, only the 2N^VS translocation from *Aegilops ventricosa* (Tausch) provides useful yet partial and environment and/or genetic background-dependent resistance to wheat blast (Cruppe et al., 2019; Cruppe et al., 2020; Cruz et al., 2016b; Valent, 2016). For that reason, scientists continue to search for new sources of resistance to wheat blast. Plant disease assessment by human raters is the standard method used for plant disease phenotyping. Humans are trained to perform visual disease evaluations, and with the experience gained, their reliability can be improved. Plant disease assessments, or phytopathometry, refers to the measurement and quantification of plant disease severity or incidence, which is essential when studying and analyzing diseases at organ, plant, or population levels (Bock et al., 2010, Large, 1966, Nutter et al., 2006). These assessments are helpful, but they are subjective evaluations that can introduce variability (Bock et al., 2020).

A digital agricultural revolution is occurring, where sensors and loggers collect data that can support growers and agricultural scientists to make better decisions. The combination of image-based sensing and machine learning frameworks has transformed many areas of research, including agriculture. In the future, machine learning and sensing technology combined with

expert knowledge, will be key to answer disease and crop yield prediction questions (Chlingaryan et al., 2018).

Digital images of diseased plants or plant organs can be used to train supervised machine learning models to classify those images in specific categories or scales in a faster, objective, and more accurate manner (Bock et al., 2020). In early 2019, a rice blast deep convolutional neural network model was trained with 5,812 Red Green Blue (RGB) images to recognize the disease under field conditions (Liang et al., 2019). Using wheat RGB field images, Alkhudaydi et al. developed a fully convolutional model to estimate the number of wheat spikelets (2019).

In addition to research under field conditions, the use of controlled conditions can speed up the identification and selection of disease-resistant candidate cultivars (Mahlein, 2015). Current plant phenotyping's main goals embrace raising consistency, accuracy, and quality of plant disease assessments and throughput of phenotype inference while reducing costs via automation (Bock et al., 2010; Rahaman et al., 2015). For this reason, reliable disease classification deep learning models need to be developed.

This document contributes new information on the wheat blast pathosystem with data collected under field and controlled-environment conditions in South America, where the disease is prevalent. It provides details on wheat blast epidemiology that can assist breeders during the selection process. It also includes developing an accurate deep learning model that can be used to classify wheat spike blast severity in three main groups under controlled conditions. The ultimate goal is to help scientists and decision-makers execute better decisions when fighting against the wheat blast disease.

1.1 References

Alkhudaydi, T., Zhou, J., & De La Iglesia, B. 2019. SpikeletFCN: Counting spikelets from infield wheat crop images using fully convolutional networks. Lecture notes in computer science.11508 LNAI, 3–13. https://doi.org/10.1007/978-3-030-20912-4_1

Aman, A. 2016. Wheat blast' threatens yield—farmers in 6 districts complain of infection. *Dailystar*. <http://www.thedailystar.net/backpage/wheat-blast-threatens-yield-784372>. Accessed 6 Jun 2020

Barea, G., & Toledo, J. 1996. Identificación y zonificación de pyricularia (*Pyricularia oryzae*) en el cultivo de trigo en el departamento de Santa Cruz. Informe Técnico, Proyecto de Investigación Trigo. 76-86.

Bhattacharya, R., & Pal, S. 2017. Deadly wheat blast symptoms enters India through the Bangladesh border, Bengal govt burning crops on war footing. *Hindustan Times*, Kolkata, Updated: Mar 05, 2017 13:52 IST <http://www.hindustan times.com/kolkata/deadly-wheat-blast-symptoms-enters-india-through-the-bangladesh-border-bengal-govt-burning-crops-on-war-footing/story-3zoWQ0H7sdMU4HxQyzWU sN.html>. Accessed August 2020.

Bock, C. H., Barbedo, J. G. A., Del Ponte, E. M., Bohnenkamp, D., & Mahlein, A.K. 2020. From visual estimates to fully automated sensor-based measurements of plant disease severity: status and challenges for improving accuracy. *Phytopathology Research*. 2(1), 1–30.

Bock, C. H., Poole, G. H., Parker, P. E., & Gottwald, T. R. 2010. Plant disease severity estimated visually, by digital photography and image analysis, and by hyperspectral imaging. *Critical Reviews in Plant Sciences*. 29(2), 59-107.

Cabrera, M. G., & Gutiérrez, S. 2007. Primer registro de *Pyricularia grisea* en cultivos de trigo del NE de Argentina. Jornada de Actualización en Enfermedades de Trigo. Buenos Aires: IFSC Press 60.

Cardoso, C.A.d.A., Reis, E. M., & Moreira, E. N. 2008. Development of a warning system for wheat blast caused by *Pyricularia grisea*. *Summa Phytopathologica*. 34, 216–221.

Chlingaryan, A., Sukkariéh, S., & Whelan, B. 2018. Machine learning approaches for crop yield prediction and nitrogen status estimation in precision agriculture: A review. *Computers and Electronics in Agriculture*. 151, 61–69. <https://doi.org/10.1016/j.compag.2018.05.012>

Cruppe, G., Silva, P., da Silva, C.L., Peterson, G., Pedley, K.F., Cruz, C.D., Asif, M., Lollato, R.P., Fritz, A.K. & Valent, B. 2020. Genome wide association reveals limited benefits of pyramiding the 1B and 1D loci with the 2N^VS translocation for wheat blast control. *Crop Science*. <https://doi.org/10.1002/csc2.20397>.

Cruppe, G., Cruz, C., Peterson, G., Pedley, K., Mohammad, A., Fritz, A., & Valent, B. 2019. Novel sources of wheat head blast resistance in modern breeding lines and wheat wild relatives. *Plant Disease*. 104, 35–43.

Cruz, C., & Valent, B. 2017. Wheat blast disease: danger on the move. *Tropical Plant Pathology*. 42, 210–222.

Cruz, C. D., Peterson, G. L., Bockus, W. W., Kankanala, P., Dubcovsky, J., Jordan, K. W., & Valent, B. 2016a. The 2N^VS translocation from *Aegilops ventricosa* confers resistance to the *triticum* pathotype of *Magnaporthe oryzae*. *Crop Science*. 56, 990–1000.

Cruz, C. D., Magarey R. D., Christie, D. N., Fowler, G. A., Fernandes, J. M., Bockus, W. W., Valent, B., & Stack, J. P. 2016b. Climate suitability for *Magnaporthe oryzae* *Triticum* pathotype in the United States. *Plant Disease*. 100, 1979–1987.

- Cruz, C. D., Kiyuna, J., Bockus, W., Todd, T. C., Stack, J. P., & Valent, B. 2015. *Magnaporthe oryzae* conidia on basal wheat leaves as a potential source of wheat blast inoculum. *Plant Pathology*. 64, 1491-1498.
- Gomes, D. P., Rocha, V. S., Rocha, J. R. A. S. C., Souza, M. A., & Pereira, O. L. 2019. Progresso temporal da brusone do trigo em função do inóculo primário, da aplicação defungicida e da resistência dos genótipos. *Summa Phytopathology*. 45, 50-58.
- Gongora-Canul, C., Salgado, J., Singh, D., Cruz, A., Cotrozzi, L., Couture, J. J., Rivadeneira, M. G., Cruppe, G., Valent, B., Todd, T., Poland, J., & Cruz, C. D. 2019. Temporal Dynamics of wheat blast epidemics and agreement between remotely sensed data measurements and visual estimations of wheat spike blast under field conditions. *Phytopathology*. 110(2):393-405.
- Goulart A.C. P, Sousa P.G., & Urashima, A.S. 2007. Damages in wheat caused by infection of *Pyricularia grisea*. *Summa Phytopathology*. 33, 358–63.
- Goulart, A., & Paiva, F. 1992. Incidência da brusone (*Pyricularia oryzae*) em diferentes cultivares de trigo (*Triticum aestivum*) em condições de campo. *Fitopatologia Brasileira*. 17:321-325.
- Igarashi, S. 1990. Update on wheat blast (*Pyricularia oryzae*) in Brazil. Pages 480-483 in Proc. Int. Conf. Wheat for nontraditional warm areas. CIMMYT, Mexico, D.F.
- Igarashi, S., Utiamada, C. M., Igarashi, L. C., Kazuma, A. H., & Lopes, R. S. 1986. Ocorrência de *Pyricularia sp.* em trigo no estado do Paraná. *Fitopatologia Brasileira*, 11: 351–352.
- Large, E.C. 1966. Measuring plant disease. Annual Review of Phytopathology. 4, 9-28.
- Liang, W.J., Zhang, H., Zhang, G. F., & Cao, H. X. 2019. Rice Blast Disease Recognition Using a Deep Convolutional Neural Network. *Scientific Reports*, 9(1).
- Madden, L. V., Hughes, G., & van den Bosch, F. 2007. The study of plant disease epidemics. *The American Phytopathological Society*.
- Mahlein, A.-K, 2015. Precision agriculture and plant phenotyping are information-and technology-based domains with specific demands and challenges for. *Plant disease*, 100(2), 241-251.
- Malaker, P. K., Barma, N. C. D., Tiwari, T. P., Collis, W. J., Duveiller, E., Singh, P. K., Joshi, A. K., Singh, R. P., Braun, H. J., Peterson, G. L., Pedley, K. F., Farman, M. L, & Valent, B. 2016. First report of wheat blast caused by *Magnaporthe oryzae* pathotype *triticum* in Bangladesh. *Plant Disease*. 100: 2330–2330.
- Mills, K. B., Salgado, J.D., Cruz, C.D., Valent, B., Madden, L. V., & Paul, P.A. 2020. Comparing the temporal development of wheat spike blast epidemics in a region of Bolivia where the disease is endemic. *Plant Disease*. Doi: 10.1094/pdis-04-20-0876-re.

- Mottaleb, K. A., Singh, P. K., Sonder, K., Kruseman, G., Tiwari, T. P., Barma, N. C. D., Malaker, P.K., Braun, H.-J., & Erenstein, O. 2018. Threat of wheat blast to South Asia's food security: An ex-ante analysis. *PLoS ONE*, 13(5). <https://doi.org/10.1371/journal.pone.0197555>
- Nutter, F.W., Esker, P.D. & Netto, R.A.C. 2006. Disease Assessment Concepts and the Advancements Made in Improving the Accuracy and Precision of Plant Disease Data. *European Journal of Plant Pathology*. 115, 95–103
- Perello, A., Martinez I., & Molina, M. 2015. First report of virulence and effects of *Magnaporthe oryzae* isolates causing wheat blast in Argentina. *Plant Disease*. 99(8):1177
- Rahaman, M. M., Chen, D., Gillani, Z., Klukas, C., & Chen, M. 2015. Advanced phenotyping and phenotype data analysis for the study of plant growth and development. *Frontiers in Plant Science*. <https://doi.org/10.3389/fpls.2015.00619>
- Tembo, B., Mulenga, R. M., Sichilima, S., M'siska, K. K., Mwale, M., Chikoti, P. C., & Braun, H. J. 2020. Detection and characterization of fungus (*Magnaporthe oryzae* pathotype *Triticum*) causing wheat blast disease on rain-fed grown wheat (*Triticum aestivum* L.) in Zambia. *PLOS ONE*, 15(9).
- Valent B. 2016. Novel strategies for managing blast diseases on rice and wheat. Progress report 01/01/15 to 12/31/15 <http://www.reeis.usda.gov/web/crisprojectpages/0231543-novel-strategies-for-managing-blast-diseases-on-rice-and-wheat.html>. Accessed August 2020.
- Viedma, L. Q. 2005. Wheat blast occurrence in Paraguay (Abstract). *Phytopathology* 95: S152.

CHAPTER 2. EPIDEMIOLOGICAL CRITERIA TO SUPPORT BREEDING TACTICS AGAINST THE EMERGING, HIGH CONSEQUENCE WHEAT BLAST DISEASE

*This chapter has been published as a research article in Plant Disease Journal
<https://doi.org/10.1094/PDIS-12-19-2672-RE>.

2.1 Introduction

Wheat Blast caused by the fungus *Magnaporthe oryzae* pathotype *Triticum* (MoT) (anamorph *Pyricularia oryzae* pathotype *Triticum*) is a significant disease and an emerging threat to global wheat production. Under favorable conditions, wheat blast can cause up to 100% yield losses (Barea and Toledo, 1996; Cabrera and Gutiérrez, 2007; Malaker et al., 2016; Viedma, 2005). MoT can infect wheat leaves and spikes (Cruz et al., 2016a; Cruz and Valent, 2017; Gomes et al., 2019; Igarashi et al., 1986). Wheat spike blast is the most visible symptom under field conditions, and the role of wheat leaf blast for spike blast development is practically unknown (Cruz et al., 2015; Cruz and Valent, 2017; Cruz et al., 2019; Góngora-Canul et al., 2019). Unfortunately, there is limited ecological and epidemiological information on this pathosystem. Under such a scenario, decision-makers struggle to develop adequate wheat blast management strategies, and consequently, farmers rely heavily on fungicide applications. In Bolivia, for example, farmers could spray around three fungicide applications at heading stage to control wheat blast (Cruz et al., 2015). However, under current guidelines, there is no compelling evidence to support general fungicide recommendations for wheat spike blast management (Cruz et al., 2019), and numerous applications at heading may not be the most cost-effective management strategy. Specific knowledge of wheat blast epidemiology, including the dynamics of inoculum buildup under different cultivar and background levels, is necessary to manage the disease. For instance, the limited epidemiological research conducted in this pathosystem has only involved one or a few susceptible cultivars (Gomes et al., 2019; Gongora-Canul et al., 2019).

An international effort has been conducted towards the identification of sources of genetic resistance to wheat spike blast (Arruda et al., 2005; Cruppe et al., 2019; Cruz et al., 2012; Cruz et al., 2016b; Goulart and Paiva, 1992; Igarashi, 1990; Martinez et al., 2019; Prestes et al., 2007; Urashima et al., 1999; Urashima et al., 2004). However, over the years, there have been limited

sources of genetic resistance to the disease, and the only effective genetic source for control is contained in the 2N^VS translocation from *Aegilops ventricosa* (Cruppe et al., 2019; Cruz et al., 2016b). In this sense, breeders have developed an excellent tactic, but without an adequate strategy, such tactic is at risk (Cruz and Valent, 2017). Boom-and-bust cycles (Priestly, 1978) appear to be frequently occurring after a period of widespread cultivation of wheat cultivars succumbing to wheat blast (Cruz et al., 2016a; Vales et al., 2018). In addition, wheat cultivars are not immune to wheat blast, and there is no known source of genetic resistance that can entirely eliminate the effects of wheat leaf blast, wheat spike blast, or both (Cruppe et al., 2019; Cruz and Valent, 2017). Plant disease epidemiology provides a better understanding of the temporal and spatial dynamics of disease intensity in host populations (Madden et al., 2007). This epidemiological information is critical for the development of integrated disease management strategies.

We hypothesize that epidemiological parameters are relevant to support wheat blast breeding tactics. To test this hypothesis, we focused on the following objective: to assess ten spring cultivars for wheat blast resistance using epidemiological parameters. To this aim, wheat leaf blast and wheat spike blast dynamics were evaluated in multiple environments.

2.2 Materials and methods

2.2.1 Locations

Experiments were carried out at two locations in Bolivia during the 2018-2019 growing season. Experiments were established on the 5 and 21 December 2018 at the Municipalities of Quirusillas and Bermejo, respectively. At each location, two experimental fields were planted and surrounded by infected seeds. However, in Quirusillas, wheat blast had been reported previously under natural conditions, not in Bermejo.

2.2.2 Genetic materials and crop management

Ten South American spring wheat cultivars with different levels of resistance to wheat spike blast (Table 1.1) were planted at 70-80 seeds per linear meter at a depth of 2-3 cm. Herbicides and insecticides were used for post-emergent management of weeds and pests based on local recommendations. Both locations relied on supplemental irrigation to promote wheat blast disease development.

Table 2.1 List of cultivars of different wheat spike blast resistance groups planted in two locations in Bolivia during the 2018-2019 season.

Number	Cultivar	Source	Wheat spike blast resistance	Data source
1	Atlax	ANAPO, Bolivia	S	Cruz et al., 2019
2	Urubó	ANAPO, Bolivia	R	Cruppe et al., 2019
3	TBIO-Sossego	ANAPO, Bolivia	MR	Cruppe et al., 2019
4	San Pablo	ANAPO, Bolivia	R	Baldelomar et al., 2015
5	AN-120	ANAPO, Bolivia	R	Cruppe et al., 2019
6	Motacú	CIAT, Bolivia	MR/MS	Cruz et al., 2016; Vales et al., 2018
7	BR-18	ANAPO, Bolivia	MR/MS	Cruz et al., 2016
8	TBIO-Mestre	Biotrigo, Brazil	MR/MS	Cruppe et al., 2019
9	TBIO-Mirante	Biotrigo, Brazil	MS	Biotrigo Genética
10	TBIO-Alvorada	Biotrigo, Brazil	S	Biotrigo Genética

S: susceptible, R: resistant, MT: moderately resistant, and MS: moderately susceptible.

2.2.3 Experimental design

Two experiments were established at each location, for a total of four environments. The experimental design was a randomized complete block with four replications as block factors and ten treatments (cultivars) randomly assigned into blocks. The experimental units (i.e., plots) measured 2 m x 2 m. Plots were separated by 1 m border rows of corn to minimize interplot interference. At each location, experiment one was surrounded by susceptible plants of the cultivar Atlax. Plants were grown from naturally MoT-infected seed from a seed lot with 10% MoT incidence (based on blotter test) and used as inoculum spreader. Meanwhile, experiment two was surrounded by moderately resistant plants of the cultivar Urubó grown from untreated seed;

however, each individual plot of the experiment was surrounded by susceptible plants of the cultivar Atlax grown from MoT-infected seed and used as a source of inoculum. Consequently, separate analyses were performed by experiment and location.

2.2.4 Visual disease assessment and grain weight

Visual assessment of severity was used to study the epidemiology of wheat leaf blast and wheat spike blast. Severity was assessed as the percentage of diseased area within individual leaf or spike. Fifteen plants per plot and their plant organs, corresponding to flag leaf (F) and the six leaves below, flag leaf – 1 (F-1), flag leaf -2 (F-2), through flag leaf -6 (F-6), and spikes (S), were individually evaluated at each assessment time. Visual estimations were taken twelve times in both experiments in Bermejo, and nine times for both experiments in Quirusillas. All plots were harvested by hand at the end of the season, and one hundred randomly selected seeds were weighed per plot ($\text{g } 100\text{-seed}^{-1}$).

2.2.5 Data analysis

The area under the disease progress curve (AUDPC) was computed using the trapezoidal integration method (Campbell and Madden, 1990). The total AUDPC (tAUDPC) was calculated considering wheat leaf blast and wheat spike blast severity data. Leaf AUDPC (lAUDPC) and spike AUDPC (sAUDPC) were calculated separately, considering wheat leaf blast and wheat spike blast severity, respectively. Repeated measurement analysis was conducted using the PROC MIXED procedure in SAS v.9.4 (SAS, Cary NC) to evaluate the effect of disease severity (converted to Arcsine root square transformation), among experiments (EXP), days after emergence (DAE), cultivars (CUL), and organ position (leaves and spike) for each location.

Graphics of untransformed y versus t or transformed y^* versus t , where $y^* = \ln(y)$, were used to characterize the temporal dynamics of wheat leaf blast and wheat spike blast severity over time. The independent variable was DAE, and the dependent variable was wheat blast expressed as wheat leaf blast or wheat spike blast severity ($y/100$, and when $y=0$ and $y=100$, were corrected as $y=+0.0001$ and $y=-0.0001$, respectively). Severity was calculated by taking the average of all the plant organs of fifteen plants per plot. Four population growth models were fitted for ten cultivars (Table 2.1) in their linearized form to describe wheat blast epidemics: exponential ($\ln[y] = \ln(y_0) + r_E$

t), logistic ($\ln[y/(1-y)] = \ln[y_0/(1-y_0)] + r_L t$), monomolecular ($\ln[1/(1-y)] = \ln[1/(1-y_0)] + r_M t$), and Gompertz ($-\ln[-\ln(y)] = -\ln[-\ln(y_0)] + r_G t$) (Cambell and Madden, 1990; Madden et al., 2007) where y_0 is the initial disease, y the amount of the disease, t is time, and r is rate of disease progress. Ordinary least squares regression was achieved with SAS v.9.4 (SAS Institute, Cary, NC) for each possible model (Campbell and Madden, 1990; Madden et al., 2007). To select the most adequate model(s) that best describe each type of epidemic we compared the following criteria: the observed and transformed disease progress curve (DPC), the coefficients of determination (R^2), the root mean square error (RMSE), and the residual errors plots versus predicted values (Campbell and Madden, 1990). Then, the delta Akaike's Information Criterion (ΔAIC) was used to compare the two best-selected models; ΔAIC contemplates the AIC of all comparing models. $AIC = N * \left(\frac{SS}{N}\right) + 2K$, where N is the number of the observations used in the model, SSE is the sum of square of the errors, and K the number of parameters, and $\Delta AIC = AIC_i - \min AIC$ (Renner-Martin et al., 2016; Mazerolle., 2006; Kaplan and Gürcan, 2018; Raji et al., 2014).

The SAS *Lsmmeans* statement was used within the PROC GLIMMIX procedure on tAUDPC, best fit model apparent infection rate ($r^* = \text{unit day}^{-1}$), final disease severity ($Y_{max} = \%$), and grain weight ($g \text{ } 100\text{-seed}^{-1}$) to obtain the contrast estimates and the associated standard error among all cultivars. This procedure was also used to detect differences in disease severity between cultivars, blocks in experiment 1 and 2 at both locations as influenced by the design of inoculum spreader by considering T-test pairwise comparison. Pearson correlation was performed to test the association between disease epidemiological parameters (tAUDPC, r_L^* , and Y_{max}) and grain weight. Linear regression between tAUDPC and grain weight was performed using PROC REG ALL procedure on SAS v.9.4 (SAS Institute, Cary, NC) to estimate grain weight loss rate per location and experiment.

2.3 Results

Wheat leaf blast and wheat spike blast symptoms occurred at different severity levels in the two experiments conducted at each location (Tables 2.2 and 3.3) (Figure 2.1). Also, there were differences in wheat blast resistance among cultivars, considering all plant organs (from leaf F-6 to S), with severity values ranging from 0 to 100%. MoT inoculum spreader location induced differences in wheat blast severity pressure. In general, the inoculum source on experiment two

induced more wheat blast severity pressure than that established on experiment one, for both locations ($p < 0.01$) (Table 2.4). The reason was that on experiment two, the susceptible Atlix plants grown from MoT-infected seed were planted closer to individual plots than the inoculum source planted around the perimeter of experiment one (Table 2.4).

Wheat blast symptoms were present in all plant organs, leaves, and spikes, at different evaluation times after crop emergence (DAE). However, in location one, there were differences in the amount of disease over time for each plant organ considered in the analysis (Table 2.2). Also, differences were found between experiments except for leaves F-6, F-2, F, and S (Table 2.2). There were differences among cultivars regarding their reaction to wheat blast on all leaves and spikes (Table 2.2). In location two, there were differences in wheat blast severity over time in all plant organs, except for leaves F-6 and F-5 (Table 2.3). Differences in wheat blast severity were found between experiments in all plant organs except for leaf F-6 (Table 2.3). There were cultivar differences in terms of their reaction to wheat leaf blast (all leaves) and wheat spike blast (Table 2.3). For both locations, there were substantial interactions among cultivar, DAE, and experiments on plant organ severity (Tables 2.2 and 2.3).

Table 2.2. Analysis of variance of repeated measurement analysis of wheat blast severity ($Pr > F$) in different plant organs in Bermejo, Bolivia, during the 2018-2019 season.

Source of variation	F-6	F-5	F-4	F-3	F-2	F-1	F	S
DAE	<0.0001	<0.0001	<0.0001	<0.0001	1.0000	<0.0001	<0.0001	<0.0001
EXP	1.0000	<0.0005	0.0046	0.0024	0.9998	0.0399	0.6821	0.2545
EXP*DAE	1.0000	<0.0001	<0.0001	<0.0001	1.0000	0.0022	0.0446	0.3397
CUL	<0.0001	<0.0001	<0.0001	<0.0001	<0.0001	<0.0001	<0.0001	<0.0001
CUL *DAE	<0.0001	<0.0001	<0.0001	<0.0001	<0.0001	<0.0001	<0.0001	<0.0001
EXP* CUL	1.0000	<0.0001	<0.0001	<0.0001	<0.0001	<0.0001	<0.0001	<0.0001
EXP* CUL *DAE	1.0000	<0.0001	<0.0001	<0.0001	<0.0001	<0.0001	0.0010	<0.0001

DAE: days after emergence, EXP: experiment, CUL: cultivar. F-6: flag leaf -6, F-5: flag leaf -5, F-4: flag leaf -4, F-3: flag leaf -3, F-2: flag leaf -2, F-1: flag leaf -1, F: flag leaf, and spikes (S).

Table 2.3. Analysis of variance of repeated measurement analysis of wheat blast severity (Pr>F) in different plant organs in Quirusillas, Bolivia, during the 2018-2019 season.

Source of variation	F-6	F-5	F-4	F-3	F-2	F-1	F	S
DAE	0.5216	0.6975	0.0121	0.0003	<0.0001	<0.0001	<0.0001	<.0001
EXP	0.8455	0.0010	0.0010	0.0284	0.0252	0.0097	0.0051	0.0011
EXP*DAE	...	0.1338	0.1056	0.0003	0.1865	0.0195	0.0195	0.1668
CUL	0.0013	<0.0001	<0.0001	<0.0001	<0.0001	<0.0001	<0.0001	<0.0001
CUL*DAE	..	0.2166	<0.0001	<0.0001	<0.0001	<0.0001	<0.0001	<0.0001
EXP*VAR	...	<0.0001	<0.0001	<0.0001	<0.0001	<0.0001	<0.0001	<0.0001
EXP*CUL*DAE	...	0.2231	<0.0001	<0.0001	<0.0001	<0.0001	<0.0001	<0.0001

DAE: days after emergence, EXP: experiment, CUL: cultivar. F-6: flag leaf -6, F-5: flag leaf -5, F-4: flag leaf -4, F-3: flag leaf -3, F-2: flag leaf -2, F-1: flag leaf -1, F: flag leaf, and spikes (S).

Table 2.4. Parameters of the pairwise comparison T-test of three susceptible cultivars for wheat blast severity in two experiments with different spreader design at two locations in Bolivia, 2018-2019.

Bermejo									
Experiment	Block	Cultivar	Experiment	Block	Cultivar	Estimate	SE	t Value	Pr > t
1	1	Atlax	2	1	Atlax	-0.13	0.019	-6.89	<.0001
		TBIO-Mirante			TBIO-Mirante	-0.11	0.020	-5.37	<.0001
		TBIO-Alvorada			TBIO-Alvorada	-0.13	0.020	-6.37	<.0001
	2	Atlax		2	Atlax	-0.11	0.020	-5.28	<.0001
		TBIO-Mirante			TBIO-Mirante	0.01	0.020	0.46	0.6436
		TBIO-Alvorada			TBIO-Alvorada	-0.07	0.020	-3.51	0.0004
	3	Atlax		3	Atlax	-0.01	0.020	-0.46	0.6474
		TBIO-Mirante			TBIO-Mirante	-0.01	0.020	-0.64	0.5233
		TBIO-Alvorada			TBIO-Alvorada	-0.02	0.020	-0.90	0.3662
	4	Atlax		4	Atlax	-0.05	0.020	-2.31	0.0211
		TBIO-Mirante			TBIO-Mirante	0.03	0.019	1.60	0.1102
		TBIO-Alvorada			TBIO-Alvorada	0.07	0.019	3.41	0.0006
Quirusillas									
1	1	Atlax	2	1	Atlax	-0.11	0.024	-4.68	<.0001
		TBIO-Mirante			TBIO-Mirante	-0.14	0.025	-5.71	<.0001
		TBIO-Alvorada			TBIO-Alvorada	-0.09	0.024	-3.72	0.0002
	2	Atlax		2	Atlax	-0.28	0.025	-11.38	<.0001
		TBIO-Mirante			TBIO-Mirante	-0.11	0.024	-4.49	<.0001
		TBIO-Alvorada			TBIO-Alvorada	-0.09	0.025	-3.64	0.0003
	3	Atlax		3	Atlax	-0.04	0.026	-1.34	0.1789
		TBIO-Mirante			TBIO-Mirante	-0.14	0.026	-5.13	<.0001
		TBIO-Alvorada			TBIO-Alvorada	-0.11	0.024	-4.69	<.0001
	4	Atlax		4	Atlax	-0.12	0.025	-4.86	<.0001
		TBIO-Mirante			TBIO-Mirante	-0.07	0.026	-2.68	0.0073
		TBIO-Alvorada			TBIO-Alvorada	-0.10	0.026	-4.08	<.0001

SE: standard error.

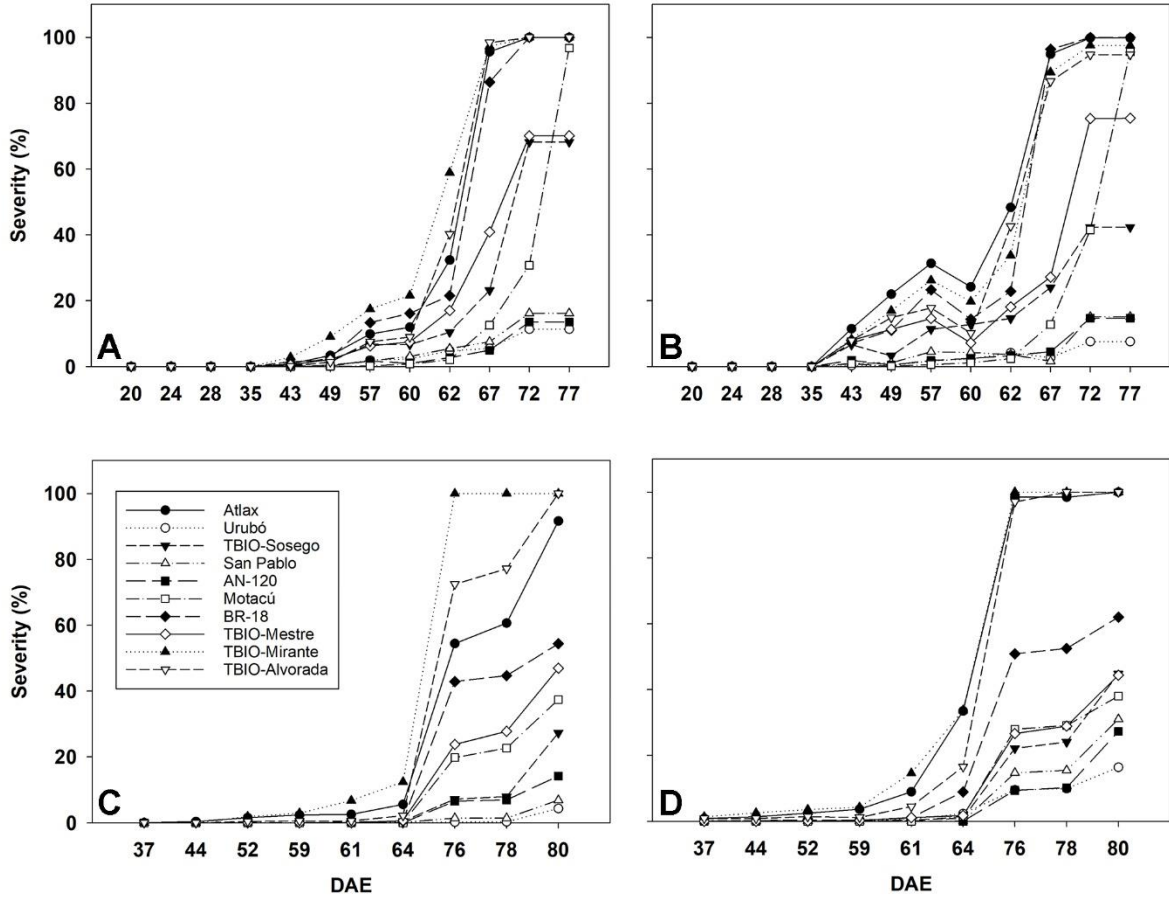


Figure 2.1. Disease progress curves for ten wheat cultivars (untransformed data y vs t (DAE: days after emergence)), in epidemics induced by *Magnaporthe oryzae* pathotype *Triticum*. Disease progress curves show the wheat leaf blast and wheat spike blast severity across all plant organs (from leaf F-6 to spike). Experiments 1 (A) and 2 (B) at Bermejo, (C) and (D) at Quirusillas conducted during the 2018-2019 growing season.

2.3.1 Temporal modeling

Ordinary least square regression performed on disease progress data for all ten cultivars by location and experiment showed that overall the logistic model provided an adequate description of wheat blast DPCs. In location one, experiment one, the logistic model best described the curves of all ten cultivars ($R^2= 0.75-0.96$; RMSE= 0.67-2.63). On experiment two, the logistic model described seven curves ($R^2= 0.88-0.93$; RMSE= 1.06-2.44), and the Gompertz model described three curves ($R^2= 0.91-0.94$; RMSE= 0.13-0.23) (Table 2.5). In location two, experiment one, the logistic model best described the curves for all 10 cultivars ($R^2= 0.63-0.92$; RMSE= 0.70-2.70). In

experiment two, the logistic model described seven curves ($R^2= 0.7-0.96$; $RMSE= 0.89-2.80$), and Gompertz described three curves ($R^2= 0.64-0.77$; $RMSE= 0.34-0.51$) (Table 2.5). The exponential and monomolecular models were deemed inadequate to describe any wheat blast progress curve based on the statistical model selection criteria.

Delta AIC (ΔAIC) for model selection between logistic and Gompertz, in location one showed that, by experiment, Gompertz had lower averages values (37.06 and 34.76) than logistic (51.18 and 56.57) for experiments one and two, respectively (Table 2.6). In location two, Gompertz had lower values (21.34 and 14.48) than logistic (39.84 and 30.40) for experiments one and two, respectively. However, the adjusted R^2 ($AdjR^2$) was higher for logistic than Gompertz. At location one, the logistic $AdjR^2$ values were 0.72-0.96 in experiment one, and 0.85-0.92 in experiment two, while the Gompertz $AdjR^2$ values were 0.45-0.92 in experiment one, and 0.52-0.94 in experiment two. At location two, the logistic $AdjR^2$ values were 0.58-0.92 experiment one, and 0.58-0.96 in experiment two, while the Gompertz $AdjR^2$ were 0.45-0.80 in experiment one, and 0.60-0.87 in experiment two (Table 2.6). Due to the above reasons for model selection criteria, logistic curves were selected to describe the temporal progress of wheat blast.

Table 2.5. Summary of statistical parameters of four linearized temporal growth models for wheat blast severity in two locations in Bolivia 2018-2019.

Location one														
Experiment one								Experiment two						
Cultivar	Model	Intercept	Slope	R ²	RMSE	Resid.	Pr>F	Model	Intercept	Slope	R ²	RMSE	Resid.	P>F
Atlax	Logistic	-18.432	0.324	0.88	2.461	S	<0.0001	Logistic	-16.646	0.292	0.93	1.666	S	<0.0001
Urubó	Logistic	-13.149	0.153	0.94	0.761	S	<0.0001	Gompertz	-2.892	0.026	0.94	0.126	S	<0.0001
TBIO Sossego	Logistic	-14.057	0.196	0.95	0.923	S	<0.0001	Gompertz	-3.375	0.046	0.94	0.230	S	<0.0001
San Pablo	Logistic	-13.681	0.162	0.93	0.923	S	<0.0001	Logistic	-12.635	0.149	0.89	1.057	S	<0.0001
AN-120	Logistic	-13.191	0.151	0.95	0.671	S	<0.0001	Gompertz	-2.964	0.029	0.91	0.181	S	<0.0001
Motacú	Logistic	-15.442	0.193	0.75	2.271	NS	0.0003	Logistic	-14.475	0.19	0.86	1.539	S	<0.0001
BR-18	Logistic	-18.571	0.322	0.87	2.577	S	<0.0001	Logistic	-17.964	0.323	0.88	2.441	S	<0.0001
TBIO- Mestre	Logistic	-14.397	0.204	0.96	0.8193	S	<0.0001	Logistic	-13.839	0.202	0.89	1.426	S	<0.0001
TBIO- Mirante	Logistic	-18.302	0.331	0.90	2.185	S	<0.0001	Logistic	-15.411	0.253	0.93	1.388	S	<0.0001
TBIO- Alvorada	Logistic	-18.922	0.331	0.87	2.627	S	<0.0001	Logistic	-15.041	0.241	0.92	1.406	S	<0.0001

Table 2.5 continued

Location two														
Experiment one								Experiment two						
Cultivar	Model	Intercept	Slope	R ²	RMSE	Resid.	Pr>F	Model	Intercept	Slope	R ²	RMSE	Resid.	P>F
Atlax	Logistic	-18.112	0.246	0.92	1.111	S	<0.0001	Logistic	-17.969	0.290	0.81	2.242	NS	0.0009
Urubó	Logistic	-15.048	0.118	0.63	1.466	NS	0.0107	Gompertz	-4.009	0.040	0.77	0.346	S	0.0017
TBIO-Sossego	Logistic	-18.502	0.204	0.87	1.250	NS	0.0002	Gompertz	-4.267	0.048	0.70	0.512	NS	0.0049
San Pablo	Logistic	-15.556	0.147	0.92	0.700	S	<0.0001	Logistic	-20.638	0.234	0.87	1.454	S	0.0002
AN-120	Logistic	-18.505	0.189	0.69	2.031	NS	0.0053	Gompertz	-4.207	0.041	0.64	0.494	NS	0.0087
Motacú	Logistic	-19.975	0.225	0.73	2.173	NS	0.0031	Logistic	-21.141	0.248	0.78	2.087	S	0.0014
BR-18	Logistic	-21.865	0.262	0.77	2.309	NS	0.0018	Logistic	-17.223	0.220	0.94	0.890	S	<0.0001
TBIO-Mestre	Logistic	-20.804	0.24	0.70	2.501	NS	0.0045	Logistic	-17.727	0.214	0.96	0.664	S	<0.0001
TBIO-Mirante	Logistic	-29.855	0.483	0.92	2.237	S	<0.0001	Logistic	-21.062	0.363	0.81	2.806	NS	0.0009
TBIO-Alvorada	Logistic	-24.480	0.351	0.81	2.704	NS	0.0009	Logistic	-20.862	0.338	0.76	3.080	NS	0.0022

RMSE: root mean square error, S: scatter, NS: no scatter, and Resid.: residual.

Table 2.6. Summary of statistical parameters and Akaike's information criterium (AIC) and delta Akaike's information criterium (Δ AIC) of linearized logistic and Gompertz models for ten cultivars at two locations in Bolivia in 2018-2019.

Location one													
Experiment one								Experiment two					
Cultivars	Model	SSE	Adj.R ²	N	K	AIC	Δ AIC	SSE	Adj.R ²	N	K	AIC	Δ AIC
Atlax	Logistic	60.56	0.87	12	2	23.43	64.66	27.75	0.92	12	2	14.06	61.93
	Gompertz	75.91	0.58	12	2	26.14	67.37	27.81	0.72	12	2	14.09	61.95
Urubó	Logistic	5.80	0.94	12	2	-4.72	36.52	5.42	0.93	12	2	-5.54	42.33
	Gompertz	0.28	0.92	12	2	-41.24	0.00	0.16	0.94	12	2	-47.87	0.00
TBIO-Sossego	Logistic	8.53	0.94	12	2	-0.10	41.14	17.40	0.88	12	2	8.46	56.32
	Gompertz	2.00	0.85	12	2	-17.47	23.77	0.53	0.94	12	2	-33.44	14.43
San Pablo	Logistic	8.52	0.92	12	2	-0.10	41.13	11.18	0.88	12	2	3.15	51.01
	Gompertz	0.45	0.90	12	2	-35.40	5.84	0.40	0.89	12	2	-36.94	10.92
AN-120	Logistic	4.51	0.95	12	2	-7.74	33.50	9.74	0.89	12	2	1.49	49.36
	Gompertz	0.31	0.91	12	2	-39.94	1.29	0.33	0.91	12	2	-39.16	8.71
Motacú	Logistic	51.57	0.72	12	2	21.50	62.73	23.67	0.85	12	2	12.15	60.02
	Gompertz	14.59	0.45	12	2	6.35	47.58	11.12	0.52	12	2	3.09	50.95
BR-18	Logistic	66.41	0.85	12	2	24.53	65.77	59.60	0.87	12	2	23.23	71.10
	Gompertz	79.65	0.55	12	2	26.71	67.95	71.84	0.59	12	2	25.47	73.34
TBIO-Mestre	Logistic	6.71	0.96	12	2	-2.97	38.27	20.34	0.88	12	2	10.33	58.20
	Gompertz	1.97	0.87	12	2	-17.70	23.53	2.37	0.85	12	2	-15.45	32.41
TBIO-Mirante	Logistic	47.78	0.89	12	2	20.58	61.82	19.27	0.93	12	2	9.68	57.55
	Gompertz	65.78	0.63	12	2	24.42	65.65	9.80	0.80	12	2	1.57	49.43
TBIO-Alvorada	Logistic	69.01	0.85	12	2	24.99	66.23	19.77	0.92	12	2	9.99	57.86
	Gompertz	77.57	0.59	12	2	26.39	67.63	7.02	0.81	12	2	-2.43	45.44

Table 2.6 continued

Location two													
Cultivars	Model	Experiment one						Experiment two					
		SSE	Adj.R ²	N	K	AIC	ΔAIC	SSE	Adj.R ²	N	K	AIC	ΔAIC
Atlax	Logistic	8.64	0.92	9	2	3.64	32.03	35.20	0.82	9	2	16.27	34.52
	Gompertz	3.50	0.78	9	2	-4.50	23.9	34.87	0.65	9	2	16.19	34.44
Urubó	Logistic	15.04	0.58	9	2	8.62	37.02	29.82	0.65	9	2	14.78	33.03
	Gompertz	0.49	0.50	9	2	-22.21	6.18	0.84	0.75	9	2	-17.35	0.90
TBIO-Sossego	Logistic	10.95	0.86	9	2	5.77	34.16	27.57	0.59	9	2	14.07	32.32
	Gompertz	0.83	0.77	9	2	-17.42	10.98	1.84	0.66	9	2	-10.31	7.94
San Pablo	Logistic	3.44	0.91	9	2	-4.66	23.73	14.80	0.85	9	2	8.48	26.73
	Gompertz	0.25	0.8	9	2	-28.39	0.00	1.26	0.76	9	2	-13.72	4.53
AN-120	Logistic	28.89	0.65	9	2	14.50	42.89	36.66	0.58	9	2	16.64	34.89
	Gompertz	1.12	0.65	9	2	-14.73	13.67	1.71	0.6	9	2	-10.95	7.30
Motacú	Logistic	33.08	0.70	9	2	15.72	44.11	30.49	0.76	9	2	14.98	33.23
	Gompertz	2.04	0.68	9	2	-9.36	19.03	1.83	0.75	9	2	-10.35	7.90
BR-18	Logistic	37.34	0.74	9	2	16.81	45.20	5.54	0.93	9	2	-0.36	17.88
	Gompertz	3.02	0.72	9	2	-5.82	22.58	1.32	0.86	9	2	-13.28	4.97
TBIO-Mestre	Logistic	43.79	0.67	9	2	18.24	46.63	3.08	0.96	9	2	-5.64	12.61
	Gompertz	2.40	0.69	9	2	-7.91	20.48	0.76	0.87	9	2	-18.25	0.00
TBIO-Mirante	Logistic	35.04	0.91	9	2	16.23	44.63	55.11	0.79	9	2	20.31	38.56
	Gompertz	53.25	0.74	9	2	20.00	48.40	52.74	0.71	9	2	19.91	38.16
TBIO-Alvorada	Logistic	51.20	0.79	9	2	19.65	48.04	66.39	0.73	9	2	21.98	40.23
	Gompertz	51.88	0.45	9	2	19.77	48.16	55.56	0.63	9	2	20.38	38.63

SSE: sum of squares of the error, Adj.R2: adjusted R2, N: number of observations used in the model, K: number of parameters.

2.3.2 Effect of cultivar resistance on disease and grain weight

According to the analysis of variance, in location one (Bermejo), both experiments showed significant differences in tAUDPC among cultivars (Table 2.7). In experiment one Urubó, San Pablo, and AN-120 (tAUDPC =157-204) had the lowest amount of disease as determined from tAUDPC, while in experiment two Urubó was the lowest, but was not significantly different from San Pablo and AN-120 (tAUDPC = 107-186). In experiment one, TBIO-Mirante had the highest level of disease, but was not significantly different from TBIO-Alvorada and Atlax (tAUDPC =1390-1687). In experiment two Atlax, BR-18, TBIO-Mirante, and TBIO-Alvorada had the highest level of disease (tAUDPC =1604-1873). The logistic apparent infection rates (r_L^*) were significantly different among cultivars in the both experiments. Urubó, San Pablo, and AN-120 had the lowest rates (0.14-0.16 unit day⁻¹), while Atlax, BR-18, TBIO-Mirante, and TBIO-Alvorada had the highest infection rate in both experiments (0.29-0.34 unit day⁻¹). For final disease severity (Y_{max}), in both experiments, the lowest severity was for cultivars Urubó, San Pablo, and AN-120 (Y_{max} = 8-17%), while cultivars Atlax, BR-18, TBIO-Mirante, Motacú, and TBIO-Alvorada had the highest values (Y_{max} = 95-100%). Grain weight loss values were different among cultivars, in both experiments, and the lowest grain weights were for Atlax, Motacú, BR-18, TBIO-Mirante, and TBIO-Alvorada (0.00 g 100-seeds⁻¹). While in experiment one, the highest grain weight was obtained with cultivar Urubó, AN-120, and San Pablo (15-17 g 100-seeds⁻¹). Similarly, in experiment two the highest grain weight was obtained with cultivar Urubó and AN-120, but were not significantly different from San Pablo (15-16 g 100-seeds⁻¹).

In location two, both experiments showed significant differences in tAUDPC among cultivars (Table 2.7). In experiment one, Urubó and San Pablo had the lowest amount of disease as determined from tAUDPC, but was not significantly different from Motacú (tAUDPC =7-222), while in experiment two, Urubó and AN-120 had the lowest amount of disease, but was not significantly different from San Pablo and TBIO-Sossego (tAUDPC = 127-306). In experiment one, TBIO-Mirante had the highest level of disease (tAUDPC =1167), and in experiment two, cultivars Atlax and TBIO-Mirante had the highest amount of disease (tAUDPC =1417-1366). The logistic apparent infection rates (r_L^*) were significantly different among cultivars in both experiments. In experiment one, Urubó and San Pablo had the lowest disease rate (0.10-0.11 unit day⁻¹), while in experiment two, TBIO-Sossego had the lowest rate, but was not significantly

different from Urubó, San Pablo, and AN-120 (0.18-0.21 unit day⁻¹). In experiment one, TBIO-Mirante had the highest infection rate (0.48 unit day⁻¹), and in experiment two, cultivars Atlax, TBIO-Alvorada, and TBIO-Mirante had the highest disease infection rate (0.35-0.37 unit day⁻¹). For final disease severity (Y_{max}), in experiment one, the lowest disease severity were for cultivars Urubó, San Pablo, and AN-120 (Y_{max} = 5-13%), while in experiment two, Urubó had the lowest severity, but was not significantly different from AN-120 (Y_{max} = 16-33%). In both experiments, Atlax, TBIO-Mirante, and TBIO-Alvorada had the highest values (Y_{max} = 93-100%). Grain weight loss values were different among cultivars, in both experiments, and the lowest grain weights were for Atlax, TBIO-Mirante, and TBIO-Alvorada (0.00-2.90 g 100-seeds⁻¹). While in experiment one, the highest grain weight was obtained with cultivar Urubó and AN-120, but was not significantly different from San Pablo, TBIO-Sossego, and TBIO-Mestre (25-29 g 100-seeds⁻¹). In experiment two, the highest grain weight was obtained with cultivar AN-120, but were not significantly different from Urubó and San Pablo (26-29 g 100-seeds⁻¹) (Table 2.7).

The tAUDPC differed by locations. Location one (Bermejo) had higher values than location two (Quirusillas). However, within each location, cultivars in each of the two established experiments followed similar trends regarding to levels of wheat blast resistance (Figure 2.2). In location one, all ten cultivars in both experiments showed different levels of lAUDPC and sAUDPC ($P= 0.0063$); leaf values were 15.31-1,443.77, and spike values were 97.28-1,553.80. In location two, lAUDPC values ranged 0.00-669.29 and sAUDPC ranged 12.05-1521.46 ($P= 0.0003$) (Figure 2.3).

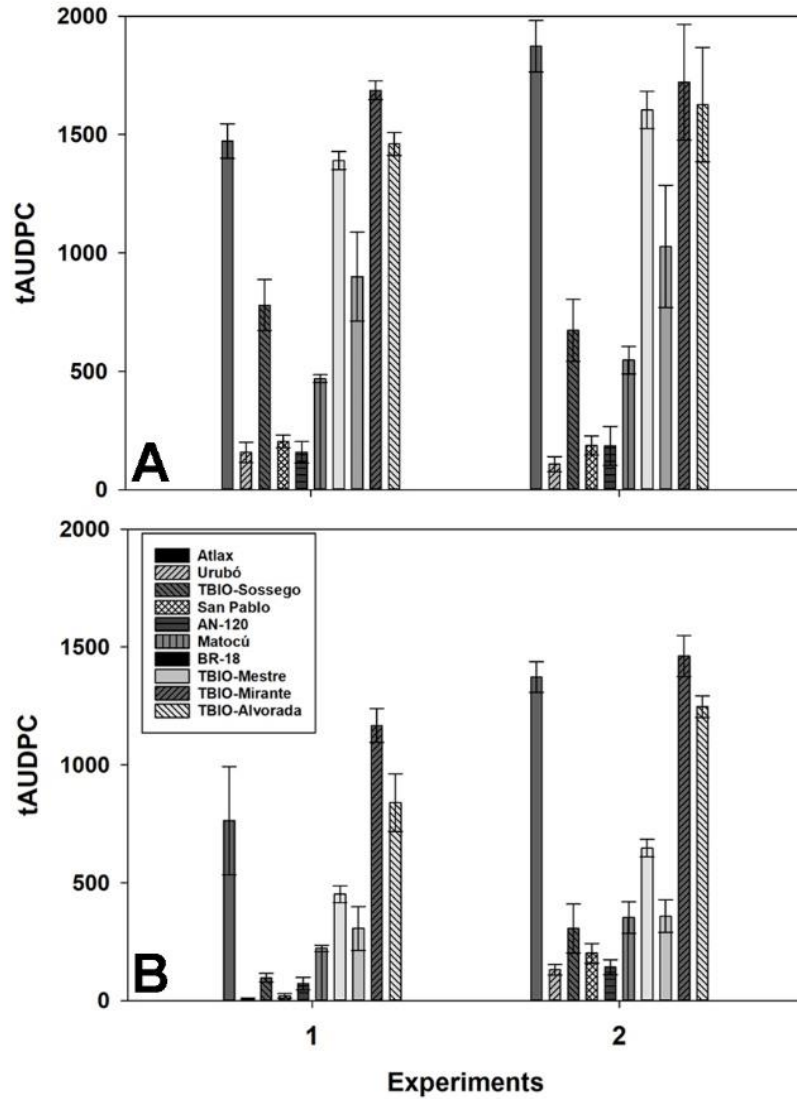


Figure 2.2. The total area under the disease progress curve of wheat leaf and spike (tAUDPC) blast of ten wheat cultivars in location one (A) according to experiments one and two. Results for location two (B) include experiment one and experiment two. Experiments were conducted in Bolivia during the 2018-2019 wheat growing season.

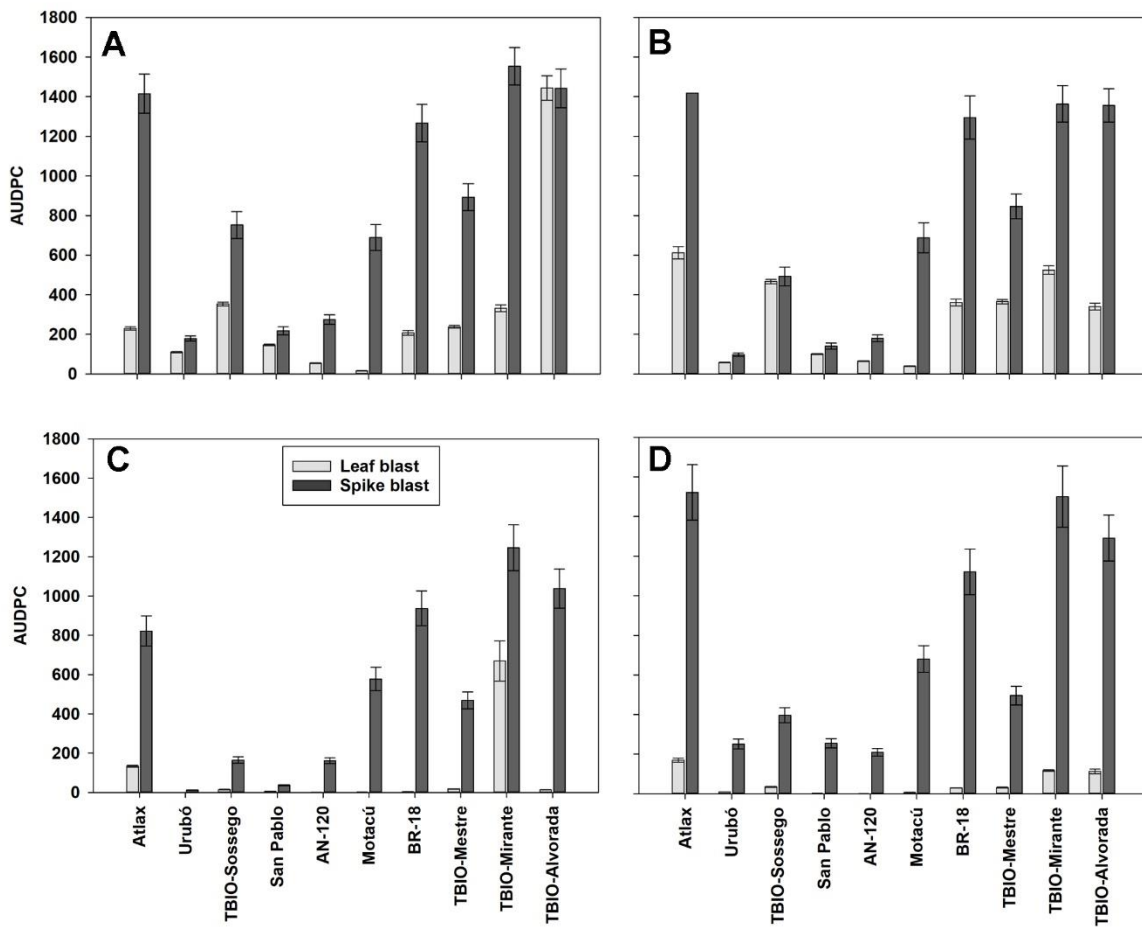


Figure 2.3. Area under the disease progress curve of wheat leaf and spike (AUDPC) blast of ten wheat cultivars in location one according to experiments one (A) and two (B). Results for location two include experiment one (C) and experiment two (D). Experiments were conducted in Bolivia during the 2018-2019 wheat growing season.

Table 2.7. Main effect of resistance (among ten cultivars) on wheat blast severity at two locations in Bolivia in 2018-2019.

Cultivar	Location one (Bermejo)							
	tAUDPC		r_L^* (unit day ⁻¹)		Y_{max} (%)		Grain weight (g 100-seeds ⁻¹)	
	Exp 1	Exp 2	Exp1	Exp 2	Exp1	Exp 2	Exp1	Exp 2
Atlax	1472.82 AB	1873.53 A	0.34 A	0.31 A	100.00 A	99.83 A	0.00 D	0.00 D
Urubó	156.91 E	107.50 E	0.15 C	0.14 C	12.49 C	7.82 D	17.49 A	16.52 A
TBIO-Sossego	779.10 C	672.97 CB	0.20 B	0.18 B	70.22 B	44.74 C	13.13 B	8.87 B
San Pablo	203.86 E	186.04 DE	0.16 C	0.14 C	17.01 C	14.98 D	15.46 AB	14.76 A
AN-120	157.39 E	184.73 DE	0.14 C	0.14 C	14.24 C	15.41 D	17.08 A	16.19 A
Motacú	468.90 D	546.42 CD	0.20 B	0.20 B	96.75 A	95.58 A	0.00 D	0.00 D
BR-18	1390.00 B	1604.28 A	0.32 A	0.33 A	100.00 A	100.00 A	0.00 D	0.00 D
TBIO-Mestre	900.44 C	1027.39 B	0.23 B	0.22 B	72.62 B	75.51 B	0.00 C	5.30 C
TBIO-Mirante	1687.23 A	1720.79 A	0.34 A	0.30 A	100.00 A	97.58 A	0.00 D	0.00 D
TBIO-Alvorada	1460.32 AB	1626.55 A	0.34 A	0.29 A	100.00 A	94.75 AB	0.00 D	0.00 D

Table 2.7 continued

Location two (Quirusillas)								
Cultivar	tAUDPC		r_L^* (unit day ⁻¹)		Y_{max} (%)		Grain weight (g 100-seeds ⁻¹)	
	Exp 1	Exp 2	Exp1	Exp 2	Exp1	Exp 2	Exp1	Exp 2
Atlax	763.63 B	1366.35 A	0.35 B	0.35 A	92.70 A	100.00 A	2.90 D	0.00 F
Urubó	6.95 E	126.63 E	0.10 E	0.18 DE	4.90 E	16.47 D	29.02 A	27.63 AB
TBIO-Sossego	97.46 D	305.96 DE	0.20 C	0.18 E	27.50 D	47.91 CB	25.20 AB	23.97 BC
San Pablo	20.41 E	283.49 DE	0.11 E	0.21 CDE	6.37 E	33.07 C	26.65 AB	25.62 ABC
AN-120	72.26 D	131.82 E	0.18 CD	0.19 DE	13.49 E	32.70 CD	28.33 A	29.00 A
Motacú	221.81 CDE	328.68 D	0.22 C	0.24 B	37.71 D	38.47 C	23.75 B	19.68 D
BR-18	451.15 C	626.02 C	0.25 C	0.22 BC	55.63 B	62.32 B	17.35 C	14.69 E
TBIO-Mestre	306.20 CD	330.83 D	0.23 C	0.22 BCD	50.44 CB	45.31 CB	25.21 AB	22.74 DC
TBIO-Mirante	1167.57 A	1416.59 A	0.48 A	0.36 A	100.00 A	100.00 A	0.00 D	0.00 F
TBIO-Alvorada	839.91 B	1191.74 B	0.41 B	0.37 A	100.00 A	100.00 A	0.00 D	0.00 F

tAUDPC: total AUDPC, r_L^* : logistic rate, and y_{max} : final disease severity.

2.3.3 Correlation among disease parameters

Significant correlations existed among disease parameters in both experiments at each of the two locations. For location one, tAUDPC, the infection rate r_L^* and Y_{max} were negatively correlated with grain weight, ($r = -0.79, -0.81, P < 0.01$), ($r = -0.81, -0.82, P < 0.01$) and ($r = -0.90, -0.96, P < 0.01$), respectively. For location two, tAUDPC, infection rate r_L^* , and Y_{max} were also negatively correlated with grain weight, ($r = -0.88, -0.95, P < 0.01$), ($r = -0.87, -0.90, P < 0.01$) and ($r = -0.89, -0.92, P < 0.01$). In location one, there were negative correlations between disease parameters, tAUDPC, r_L^* , and Y_{max} ($P < 0.05$) (Table 2.8).

Regression between grain weight and tAUDPC to predict grain weight loss, showed that slope coefficient as estimator of grain weight loss, was higher in location two (Quirusillas) (-0.021, -0.025 g-1) than in location one (Bermejo) (-0.008, -0.010 g-1) for each unit of tAUDPC (Figure 2.4).

Table 2.8. Pearson correlation coefficients for total area under the disease progress curve (tAUDPC), linearized logistic infection rate of disease progress (r_L^*), final wheat blast disease severity (Y_{max}), grain weight, in two locations in Bolivia, 2018-2019.

Location one (Bermejo)								
Experiment one					Experiment two			
	tAUDPC	r_L^* (day ⁻¹)	Y_{max} (%)	Grain weight (g 100-seeds ⁻¹)	tAUDPC	r_L^* (day ⁻¹)	Y_{max} (%)	Grain weight (g 100-seeds ⁻¹)
tAUDPC	...	0.972**	0.861**	-0.791**	...	0.951**	0.852**	-0.818**
r_L^* (unit day ⁻¹)		...	0.851**	-0.816**		...	0.864**	-0.828**
Y_{max} (%)			...	-0.906**			...	-0.963**
Grain weight (g 100-seeds ⁻¹)			
Location two (Quirusillas)								
Experiment one					Experiment two			
	tAUDPC	r_L^* (per unit day ⁻¹)	Y_{max} (%)	Grain weight (g 100-seeds ⁻¹)	tAUDPC	r_L^* (per unit day ⁻¹)	Y_{max} (%)	Grain weight (g 100-seeds ⁻¹)
tAUDPC	...	0.959**	0.912**	-0.888**	...	0.930**	0.940**	-0.951**
r_L^* (per unit day ⁻¹)		...	0.926**	-0.873**		...	0.880**	-0.908**
Y_{max} (%)			...	-0.898**			...	-0.920**
Grain weight (g 100-seeds ⁻¹)			

ns: non-significant, **: p<0.01, and *: p<0.05.

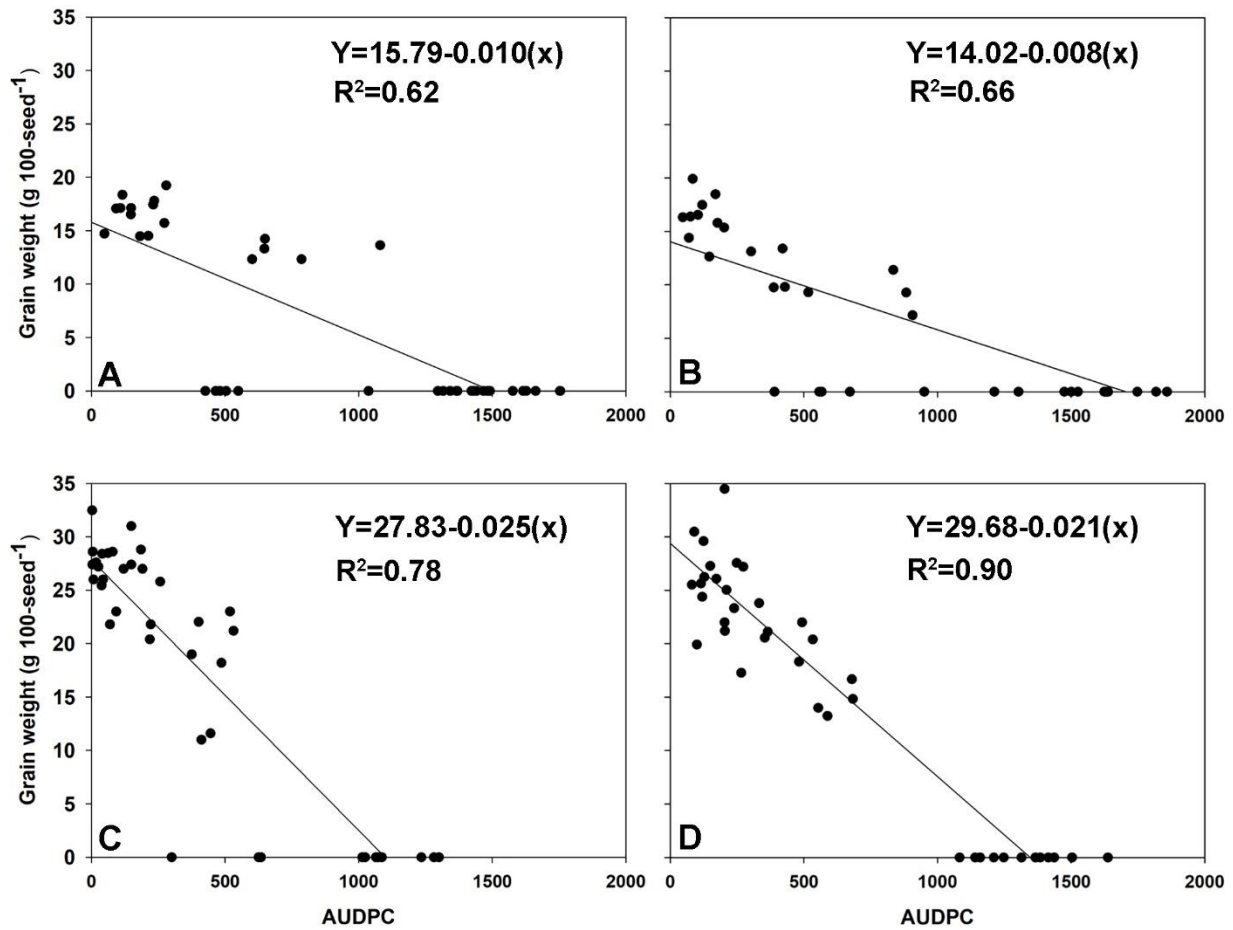


Figure 2.4. Linear regression between grain weight and wheat blast severity of ten cultivars, (A) and (B) experiments in location one (Bermejo), (C), and (D) experiments in location two (Quirusillas). Experiments were conducted in Bolivia during the 2018-2019 wheat growing season.

2.4 Discussion

This study provides clear evidence of the relevance of plant disease epidemiological criteria to support breeding tactics against wheat blast. As a starting point, cultivar resistance levels influenced the dynamics of wheat leaf blast and wheat spike blast development in various environments. In addition, epidemiological parameters associated with wheat blast resistance were critical for selection and deployment of germplasm. In general, wheat blast symptoms developed overtime on all plant organs, starting from the lower canopy in all cultivars. At both locations, there were differences in disease severity between experiments. These differences were likely due

to the distance between the MoT inoculum source and individual plots. According to Salgado et al. (unpublished) MoT infections initially develop at the lower canopy, where leaf blast severity reaches higher values compared to upper canopy leaves. This might be due to the early senescence of lower leaves caused by MoT infections (Góngora-Canul et al., 2019). In addition, a massive influx of MoT conidia from the lower canopy and subsequent compounding secondary infection cycles in the upper canopy may have occurred and caused high wheat blast severity (Góngora-Canul et al., 2019; Salgado et al., unpublished).

Regardless of environment, the logistic model best described wheat blast progress. In both locations, the logistic model described 17 out of 20 DPCs (85%) and the Gompertz model described 3 out of 20 (15%). Similar results were found by Góngora et al., (2019) and Mohapatra et al., on a rice blast study, (2008). Δ AIC for model selection showed that Gompertz had lower values than the logistic model in all experiments, but the logistic model had higher AdjR² values. The latter indicated that the logistic model better fit the data. The AdjR² values alone can consistently choose complex models compared to selection based on AIC values, and those models can reproduce better empirical datasets than those chosen by AIC (Gayawan and Ipinomo, 2009). For those reasons, the logistic model was deemed more adequate and selected to describe the temporal progress of wheat blast.

In both locations, there were significant differences in tAUDPC of blast severity among the 10 spring wheat cultivars evaluated. Cultivars Urubó, San Pablo and TBIO Sossego had the lowest, and cultivars Atlax, TBIO-Mirante and TBIO-Alvorada had the highest values of tAUDPC, respectively. The apparent infection rate, (r_L^*) (units day⁻¹) of linearized logistic model was low for cultivars Urubó, San Pablo and TBIO-Sossego and the higher r_L^* were for Atlax, TBIO-Mirante and TBIO-Alvorada. In general, more tAUDPC led to higher apparent infection rates; however, cultivar Motacú was the exception. This cultivar had low values of tAUDPC, but high r_L^* , because it provided sufficient resistance to wheat leaf blast but not enough for wheat spike blast (Figure 2.3). This early maturity cultivar, which became popular in Bolivia over the last few years (Vales et al., 2018), is known for its moderate to insufficient wheat spike blast resistance reaction, which can vary by location and season (Cruz et al., 2016a; Vales et al., 2018). This was the only case in which low tAUDPC not necessary implied a lower r_L^* .

Pratt et al. (1993) reported that AUDPC was more important for cultivar selection than rate, since AUDPC as a measure of quantitative disease resistance entails repeated disease assessment.

However, Jeger and Viljanen-Rollinson, (2001) mentioned that the effect of resistance should be expressed in terms of rate parameter ('rate-reducing' effect) and not based on the asymptotic level of disease (maximum amount of disease level without increase) in adult plants. Fry (1978) reported that AUDPC is more reliable than r^* and final disease severity (Y_{max}) for describing cultivar resistance, arguing that Y_{max} was useful only if epidemic did not progress to completion or near completion by the end of the season, and that r^* is influenced by weather. Regarding Y_{max} , cultivars Urubó, AN-120 and San Pablo had the lowest values, up to 4.9% severity. Atlax, TBIO-Mirante and TBIO-Alvorada cultivars had values of up to 100% severity. The general trend is that a higher Y_{max} , the higher AUDPC and r_L^* . Final disease severity evaluation is a practical and cheap estimator when many cultivars are being evaluated for resistance. However, using final disease severity alone could be risky if disease pressure is not high and temporal dynamics are not understood in terms of disease onset and temporal rates of progress, as it was the example of cultivar Motacú discussed above. There were significant differences in grain weight (g 100-seeds⁻¹). Overall, cultivars in location one had less grain weight than in location two. Cultivars that had low or zero grain weight were Atlax, TBIO-Mirante and TBIO-Alvorada, and cultivars with higher grain weight were Urubó, AN-120 and San Pablo. The reduction of grain weight affected by disease severity (tAUDPC, r_L^* and Y_{max}) was due to reduction of leaf green area in early phases of the epidemic and by the infection of the spike resulting in no grain formation or shriveled grain.

Differences were observed among cultivars in their combined reaction to wheat leaf blast and wheat spike blast, in both locations. Cultivars that had lowest tAUDPC such as Urubó, San Pablo and TBIO-Sossego, had the lowest lAUDPC and sAUDPC, respectively. Susceptible cultivars such Atlax, TBIO-Mirante and TBIO-Alvorada had the highest tAUDPC as well as the lAUDPC and sAUDPC respectively. In contrast, cultivar Motacú had the lowest lAUDPC but not the lowest sAUDPC. Differences in reaction to wheat blast according to plant age and organs have been previously reported (Cruppe et al., 2019; Cruz et al., 2012; Martinez et al., 2019). Wheat blast disease can be found in spike and leaf organs, and weak correlations have been reported between seedling and adult plant resistance across multiple cultivars (Cruppe et al., 2019; Cruz et al., 2012; Maciel et al., 2014). Different mechanisms for wheat blast resistance (Cruz and Valent, 2017) might exist in leaves and spikes of cultivar Motacú.

There were significant ($P < 0.01$) positive correlations among tAUDPC, apparent infection rates (r^*) and final disease severity (Y_{max}) in both locations, indicating differences in resistance

among cultivars. However, the correlation was higher between tAUDPC and r_L^* , than tAUDPC and Y_{max} . This indicated that tAUDPC or r^* can be chosen for cultivar selection in a wheat blast breeding program. However, Y_{max} could be a cheap and easy estimator, since tAUDPC and r_L^* are tedious and labor intensive due to repeated measurements are needed (Smith et al., 1998). tAUDPC, r_L^* and Y_{max} had significant negative correlations with grain weight (g 100 seeds⁻¹) at both locations ($r > 0.79$) ($P < 0.01$). However, Y_{max} had the highest correlation with grain weight, indicating that it can be used as a predictor in a single-point grain-weight loss model (critical-point) for wheat blast since it requires less data over time. tAUDPC and r_L^* can also be used as predictors in a multiple-point grain-weight loss wheat blast model (multiple-point); however, they require several disease assessments over time, and that may not be in feasible in some cases. Multiple-point models are usually more accurate than critical-point models because of their more thorough description of the epidemic (Madden, 1983).

The development and release of new cultivars occur in the face of multiple breeding objectives such as improved yield, quality, disease and drought resistance. In certain countries, the selection of newly released cultivars is less based on resistance to blast than on early maturity (Vales et al., 2018). Motacú, an early maturity cultivar was preferred in Bolivian breeding programs, although it had insufficient resistance levels to wheat spike blast. The decision to deploy Motacú was risky because the wheat blast temporal dynamics were not understood at the time of selection. Today we understand that this widely deployed cultivar in Bolivia is characterized by moderate to insufficient wheat spike blast resistance, which can vary depending on location and year. Wheat cultivars resistant to wheat leaf blast can help reduce the rate of wheat blast epidemics. Cultivars with better performance for both wheat leaf blast and wheat spike blast resistance should be preferred over those that only perform well for either leaf blast or spike blast. There is evidence that 2N^VS-based cultivars are not immune to wheat spike blast but this translocation provides cultivars some ability to deal with a given MoT load (Cruz et al., 2016b).

This is the first study that provides evidence that germplasm with different resistance background can influence the dynamics of wheat leaf blast and wheat spike blast development under multiple environments. Moreover, this study provides enough evidence and strongly supports the use of epidemiological parameters such as AUDPC, r_L^* and Y_{max} , which could be used to help pathologists and breeders better select germplasm for wheat blast resistance. Given

the threat of the introduction of the disease to new areas of the world, a better epidemiological understanding of wheat blast development on novel genetic resources is needed.

2.5 References

- Arruda, M., Bueno, C., Zamprogno, K., Lavorenti, N., & Urashima, A. 2005. Reação do trigo à *Magnaporthe grisea* nos diferentes estádios de desenvolvimento. *Fitopatologia Brasileira*. 30:121-126.
- Baldelomar, D., Cardenas, S., & Quispe, K. 2015. Caracterización de genotipos de trigo (*Triticum aestivum*) con resistencia a piricularia durante el verano 2014/2015 en Quirusillas, Santa Cruz, Bolivia. INIAF (online) vol.1, n.6, pp. 17-21. ISSN 2308-250X.
- Barea, G., & Toledo, J. 1996. Identificación y zonificación de piricularia o bruzone (*Pyricularia oryzae*) en el cultivo del trigo en el dpto. de Santa Cruz. CIAT. Pages 76–86. In: Informe Técnico. Proyecto de Investigación Trigo, Santa Cruz, Bolivia.
- Campbell, C. L., & Madden, L. V. 1990. Introduction to plant disease epidemiology. *John Wiley and Sons*. New York.
- Cabrera, M. G., & Gutiérrez, S. 2007. Primer registro de *Pyricularia grisea* en cultivos de trigo del NE de Argentina. In: Jornada de Actualización en Enfermedades de Trigo. IFSC Press, Lavallol, Buenos Aires, Argentina.
- Cruppe, G., Cruz, C. D., Peterson, G., Pedley, K., Asif, M., Fritz, A., Calderon, L., Lemes da Silva, C., Todd, T., Kuhnem, P., Singh, P. K., Singh, R. P., Braun, H., Barma, N. C. D., & Valent, B. 2019. Novel sources of wheat head blast resistance in modern breeding lines and wheat wild relatives. *Plant Disease*. 104: 35-43. doi.org/10.1094/PDIS-05-19-0985-RE.
- Cruz, C. D., Bockus, W. W., Stack, J. P., Tang, X., Valent, B., Pedley, K. F., & Peterson, G. L. 2012. Preliminary assessment of resistance among U.S. wheat cultivars to the *Triticum* pathotype of *Magnaporthe oryzae*. *Plant Disease*. 96, 1501–1505. <https://doi.org/10.1094/PDIS-11-11-0944-RE>.
- Cruz, C. D., Kiyuna, J., Bockus, W. W., Todd, T. C., Stack, J. P., & Valent, B. 2015 *Magnaporthe oryzae* conidia on basal wheat leaves as a potential source of wheat blast inoculum. *Plant Pathology*. 64: 1491–1498.
- Cruz, C. D., Magarey R. D., Christie, D. N., Fowler, G. A., Fernandes, J. M., Bockus, W. W., Valent, B., & Stack, J. P. 2016a. Climate suitability for *Magnaporthe oryzae* *Triticum* pathotype in the United States. *Plant Disease*. 100: 1979–1987. <https://doi.org/10.1094/PDIS-09-15-1006-RE>.
- Cruz, C. D., Peterson, G. L., Bockus, W. W., Kankanala, P., Dubcovsky, J., Jordan, K. W., Akhunov, E., Chumley, F., Baldelomar, F. D., & Valent, B. 2016b. The 2N^VS translocation from

Aegilops ventricosa confers resistance to the *Triticum* Pathotype of *Magnaporthe oryzae*. *Crop Science*. 56: 990–1000. <https://doi.org/10.2135/cropsci2015.07.0410>.

Cruz, C. D., & Valent, B. 2017. Wheat blast disease: danger on the move. *Tropical plant pathology*. 42: 210. <https://doi.org/10.1007/s40858-017-0159-z>.

Cruz, C. D., Santana, F. M., Todd, T. C., Maciel, J. L. N., Kiyuna, J., Baldelomar, D. F., Cruz, A. P., Lau, D., Seixas, C. S., Goulart, A. C. P., Sussel, A. A., Schipanski, C. A., Chagas, D. F., Coelho, M., Montecelli, T. D. N., Utiamada, C., Custódio, A. P., Rivadeneira, M. G., Bockus, W. W., & Valent, B. 2019. Multi-environment assessment of fungicide performance for managing wheat head blast in Brazil and Bolivia. *Tropical plant pathology*. 44:183-191.

Fry, W. E. 1978. Quantification of general resistance of potato cultivars and fungicide effects for integrated control of potato late blight. *Phytopathology*. 68:1650-1655.

Gayawan, E., & Ipinoyomi, R. A. 2009. A Comparison of Akaike, Schwarz and R Square criteria for model selection using some fertility models. *Australian Journal of Basic and Applied Sciences*. 3:3524-3530.

Gomes, D. P., Rocha, V. S., Rocha, J. R. A. S. C., Souza, M. A., & Pereira, O. L. 2019. Progresso temporal da brusone do trigo em função do inóculo primário, da aplicação defungicida e da resistência dos genótipos. *Summa Phytopathology*. 45: 50-58.

Gongora-Canul, C., Salgado, J., Singh, D., Cruz, A., Cotrozzi, L., Couture, J. J., Rivadeneira, M. G., Cruppe, G., Valent, B., Todd, T., Poland, J. & Cruz, C. D. 2019. Temporal Dynamics of wheat blast epidemics and agreement between remotely sensed data measurements and visual estimations of wheat spike blast under field conditions. *Phytopathology*. 110(2):393-405 <https://doi.org/10.1094/PHYTO-08-19-0297-R>.

Goulart, A., & Paiva, F. 1992. Incidência da brusone (*Pyricularia oryzae*) em diferentes cultivares de trigo (*Triticum aestivum*) em condições de campo. *Fitopatologia Brasileira*. 17:321-325.

Igarashi, S., Utiamada, C. M., Igarashi, L. C., Kazuma, A. H., & Lopes, R. S. 1986. *Pyricularia* em trigo. 1. Ocorrência de *Pyricularia sp.* no estado do Paraná. *Fitopatologia Brasileira*. 11:351–352.

Igarashi, S. 1990. Update on wheat blast (*Pyricularia oryzae*) in Brazil. Pages 480-483 in: Proc. Int. Conf. Wheat for nontraditional warm areas. D. Saunders, eds. *CIMMYT*, Mexico, D.F.

Jeger, M. J., and Viljanen-Rollinson, S. L. H. 2001. The use of the area under the disease-progress curve (AUDPC) to assess quantitative disease resistance in crop cultivars. *Theoretical and Applied Genetics*. 102:32-40.

Kaplan, S., & Gürcan, E. K. 2018. Comparison of growth curves using non-linear regression function in Japanese quail. *Journal of Applied Animal Research*. 46:112-117.

- Maciel, J. L. N., Ceresini, P. C., Castroagudin, V. L., Zala, M., Kema, G. H. J., & McDonald, B. A. 2014. Population structure and pathotype diversity of the wheat blast pathogen *Magnaporthe oryzae* 25 years after its emergence in Brazil. *Phytopathology* 104:95-107.
- Madden, L. V. 1983. Measuring and modeling crop losses at the field level. *Phytopathology* 73:1591-1596.
- Madden, L. V., Hughes, G., & van den Bosch. 2007. The study of plant disease epidemics. APS Press, St. Paul, MN.
- Malaker, P. K., Barma, N. C. D., Tiwari, T. P., Collis, W. J., Duveiller, E., Singh, P. K., Joshi, A. K., Singh, R. P., Braun, H. J., Peterson, G. L., Pedley, K. F., Farman, M. L., & Valent, B. 2016. First report of wheat blast caused by *Magnaporthe oryzae* pathotype *triticum* in Bangladesh. *Plant Disease*. 100: 2330–2330.
- Martinez, S. I., Sanabria, A., Fleitas, M. C. Consolo, V. F., & Perello, A. 2019. Wheat Blast: Aggressiveness of isolates of *Pyricularia oryzae* and effect on grain quality. *Journal of King Saud University*. 31: 150-157.
- Mazerolle, M. J. 2006. Improving data analysis in herpetology: using Akaike's Information Criterion (AIC) to assess the strength of biological hypotheses. *Amphibia-Reptilia* 27: 169-180.
- Mohapatra, N. K., Mukherjee, A. K., Suriya Rao, A. V., & Nayak, P. 2008. Disease progress curve in the rice pathosystem compared with the logistic and Gompertz model. *ARPN Journal of Agricultural and Biological Science*. 3:28-37.
- Pratt, R. C., Adipala, E., & Lipps, P. E. 1993. Characterization of race-nonspecific resistance to *Exserohilum turcicum* Races 0 and 1 in Maize OhS10 S₁ Progenies. *Plant Disease*. 77: 1227-1232.
- Prestes, A., Arendt, P., Fernandes, M., & Scheeren, P. 2007. Resistance to *Magnaporthe grisea* among Brazilian wheat genotypes. Pages 119-133 in: Wheat production in stressed environments. H. T. Buck, J. E. Nisi, and N. Salomón eds. Springer. Mar del Plata, Argentina.
- Priestley, R.H. 1978. Detection of increased virulence in populations of wheat yellow rust. Pages 64. In: Plant Disease Epidemiology, P. R. Scott, and A. Bainbridge eds. Blackwell, Oxford.
- Raji, C. A., Tarzwell, R., Pavel, D., Schneider H., Uszler, M., Thornton, J., van Lierop, M., Cohen, P., Amen D. G., & Henderson, T. 2014. Clinical utility of SPECT neuroimaging in the diagnosis and treatment of traumatic brain injury: a systematic review. *PloS One*, 9, e91088.
- Renner-Martin, K., Kühleitner, M., Brunner, N., & Hagemüller, W. 2016. AIC-based selection of growth models: The case of piglets from organic farming. *Open Journal of Modelling and Simulation*. 4: 17-23.
- Smith, V. L., Campbell, C. L., Jenkins, S. F., & Benson, D. M. 1998. Effect of host density and number of disease foci on epidemics of southern blight of processing carrot. *Phytopathology*. 78: 595-600.

Urashima, A. S., Hashimoto, Y., Don, L. D., Kusaba, M., Tosa, Y., Nakayashiki, H., & Mayama, S. 1999. Molecular analysis of the wheat blast population in Brazil with a homologue of retrotransposon MGR583. *Annual Phytopathology Society Japan*. 65: 429-436.

Urashima, A., Lavorenti, N. A., Goulart, A. C. P., & Mehta, Y. R. 2004. Resistance spectra of wheat cultivars and virulence diversity of *Magnaporthe grisea* isolates in Brazil. *Fitopatologia Brasileira*. 29: 511-518.

Vales, M., Anzoátegui, T., Huallpa, B., & Cazon, M. I. 2018. Review on resistance to wheat blast disease (*Magnaporthe oryzae* *Triticum*) from the breeder point-of-view: use of the experience on resistance to rice blast disease. *Euphytica*. 214:1 doi.org/10.1007/s10681-017-2087-x.

Viedma, L. Q. 2005. Wheat blast occurrence in Paraguay (Abstract). *Phytopathology* 95: S152.

CHAPTER 3. WHEAT SPIKE BLAST IMAGE CLASSIFICATION USING DEEP CONVOLUTIONAL NEURAL NETWORKS

*This chapter will be submitted as a research article.

3.1 Introduction

Wheat blast is a disease caused by the fungus *Magnaporthe oryzae Triticum* (MoT). MoT infects leaves and spikes of wheat, but wheat spike blast is the most remarkable symptom of this disease (Cruz et al., 2015; C. Cruz & Valent, 2017; Ceresini et al., 2019). Wheat blast is present in South America and South Asia, particularly in locations where warm temperatures 25-30°C, long wetness duration (25 to 40h), and high relative humidity (>90%) are predominant (Cardoso & Moreira, 2008; Igarashi et al., 1986). Recently, MoT was reported in Zambia, Africa (Tembo et al., 2020). Under conducive field conditions, the fungus can kill up to 100% of susceptible wheat spikes in a period of 2.5 to 3 weeks (Gongora-Canul et al., 2020). The search for wheat spike blast resistance sources has been intense since 1985 when the disease was first detected (Cruppe et al., 2020; Cruz et al., 2016a; Igarashi et al., 1986; Prestes et al., 2007; Urashima et al., 2004). However, only limited wheat germplasm has been tested. To date, the only useful source of genetic resistance for wheat spike blast is contained in the 2N^VS translocation from the wild wheat relative, *Aegilops ventricosa* (Cruz et al., 2016a, Cruppe et al., 2020). Obtaining tissue samples from phenotyped wheat entries and testing for the presence or absence of the 2N^VS segment is relatively easy and routine (Cruppe et al., 2019; Cruz et al., 2016a). Nevertheless, given that there is evidence that 2N^VS-based resistance may be overcome sooner or later, additional sources of wheat spike blast resistance should be identified (Cruppe et al., 2019; Cruppe et al., 2020; Cruz et al., 2016a). A bottleneck in the identification of novel sources of resistance is measuring disease intensity (i.e., plant disease phenotyping), which is considered a limiting factor in the assessment of genotype performance in plant breeding programs (Mahlein, A.-K, 2015; Sakoor et al., 2017). Therefore, innovative and transformative solutions for quantification of plant disease symptoms at the individual and host population levels are needed (Camargo et al., 2009; Kumar et al., 2020). Implementation of advanced phenotyping platforms could reduce the phenotyping bottleneck during breeding and enhance the understanding of genotype-phenotype relationships (Sakoor et al., 2017). Currently, phenotyping of wheat spike blast disease severity relies on visual estimation

made by humans (Cruz et al., 2016b). Due to issues associated with agreement in data acquisition, inter-rater agreement among other statistical tests have been used to compare the consensus or agreement between raters' estimations of disease severity (Bock et al., 2010, 2020; Madden et al., 2007; Nutter et al., 1993). Reliable disease estimations, paired with corresponding images of diseased wheat spikes, can be used as input for deep learning models. In the future, automated image analysis systems, together with deep learning models, might enable considerable increases in the throughput of trait measurements by offsetting the phenotyping bottleneck (Barbedo, 2016).

In recent years, computer vision and machine learning have emerged as new approaches to develop plant phenotyping platforms. Recent developments in machine learning have more focus on deep learning, a branch of machine learning inspired by the functions of the human brain called a neural network. The most frequently used method of deep learning for image classification are Deep Convolutional Neural Networks (DCNN). Recent studies have further enhanced the scope for using a deep-learning-based approach for classifying, identifying, and quantifying plant diseases (Singh et al., 2018).

A variety of DCNN classification models are available for plant diseases such as those developed for bacterial pustule (*Xanthomonas axonopodis* pv. *glycines*), sudden death syndrome (SDS, *Fusarium virguliforme*), Septoria brown spot (*Septoria glycines*), bacterial blight (*Pseudomonas savastanoi* pv. *glycinea*), and several abiotic stresses in soybean (Ghosal et al., 2018). In tomato (*Lycopersicon esculentum*), deep learning models were developed with and without pre-training models with images from nine leaf tomato diseases from the website www.PlantVillage.org, obtaining better performance using pre-training models (Brahimi et al., 2018). A total of 54,306 leaf images from several crops with 26 diseases were obtained from PlantVillage.org and trained using AlexNet and GoogleLeNet pre-trained models with a leaf segmented dataset, obtaining an accuracy of 99.35 % (Mohanty et al., 2016). On wheat, an in-field automatic diagnosis system for powdery mildew (*Blumeria graminis* f. sp. *tritici*), smut (*Urocystis agropyri*), leaf blotch (*Septoria tritici*), black chaff (*Xanthomonas campestris* pv. *undulosa*), stripe rust (*Puccinia striiformis* f. sp. *tritici*), and leaf rust (*Puccinia recondita* f. sp. *tritici*) was developed using deep learning and multiple instance learning techniques from the Wheat Disease Database 2017 (Lu et al. 2017). Although this database is a significant contribution for wheat disease identification based on images (labeled by agronomist experts), aspects regarding reliability of the labeler (ground truth) may be compromised (Lobet, 2017). It is necessary that detection and

quantification studies of plant disease provide evidence of ground truth estimation's agreement analysis before using the labeled images as dataset for training deep learning models. Without such information, results can be inconsistent.

We hypothesize that deep convolutional neural networks models can be trained for wheat spike blast severity image classification for pre-screening of wheat blast cultivar resistance under a controlled environment. To test this hypothesis, we focused on the following objectives:

- i) Generate a wheat spike blast image library labeled with disease severity
- ii) Analyze the agreement of the disease severity's model training set between two experts in plant pathology and an image software
- iii) Develop an accurate deep convolutional neural network model to detect and classify wheat spike blast symptoms in three severity categories.

3.2 Materials and methods

3.2.1 Plant cultivation and genetic materials

Two experiments were conducted under controlled conditions in a growth room at the Asociación de Productores de Oleaginosas y Trigo (ANAPO) research facility in Santa Cruz de la Sierra, Bolivia. Wheat cultivars were planted in pots of 15 cm diameter, filled with 3/4 vermicast and 1/4 silt, and grown at 18-25°C, 14 h light/10 h dark photoperiod, and 60% relative humidity. Plants were fertilized, and insecticide treatments were sprayed when needed. Plants were arranged in a randomized complete block design with six wheat cultivars having various levels of resistance to MoT (Fernández-Campos et al., 2020), two inoculation levels (inoculated and non-inoculated), and four replicates (Table 3.1). Wheat cultivars used in this study included South American spring cultivars Atlax, BR-18, Motacú, Urubó, AN-120, and San Pablo (Table 3.1) (Baldelomar et al., 2015; Fernández-Campos et al., 2020).

Table 3.1. Final wheat spike blast severity (Y_{max}) of wheat cultivars assessed at 19 days after inoculation

Cultivar	Atlax	BR-18	Motacú	Urubó	AN-120	San Pablo
Y_{max} (%)	100	8.69	3.75	1.88	3.31	32.88

3.2.2 Inoculation

Plants were inoculated at the growth stage Feekes 10.5 with MoT isolate 008-C (Fig. 3.1a) according to a modified inoculation protocol (C. D. Cruz et al., 2016b). A conidial suspension was adjusted to 20,000 spores/ml, and each spe received 1mL of the spore suspension. Immediately after the spikes were sprayed with the MoT inoculum, plants were moved to a dew chamber (Fig. 3.1b) to induce MoT infection (i.e., 24-26°C, 95-98% RH, and 14h light photoperiod). Forty-eight hours after inoculation, plants were removed from the dew chamber and left under controlled environment room conditions (24-26°C and relative humidity of 50-60%), until the end of the experiment.

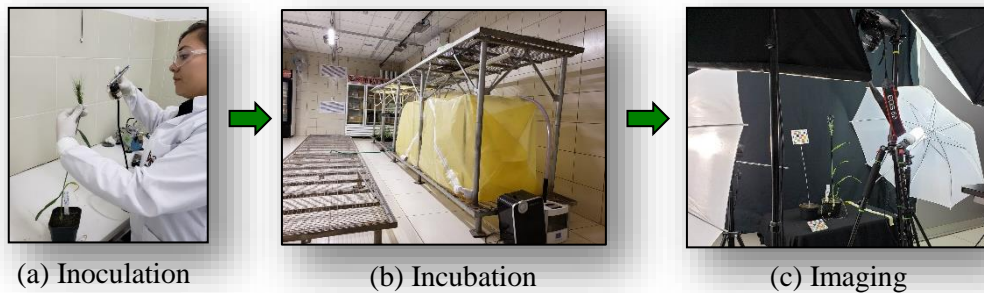


Figure 3.1. Flow process: (a) *Magnaphorthe oryzae* pathotype *Triticum* inoculation, (b) dew chamber provided optimal conditions for fungal infection, and (c) wheat spike imaging

3.2.3 Data collection

Following phytopatometry terminology, we used the term estimate for visual disease estimations made by humans and the term measurement for estimations made by image analysis (Bock et al., 2010; Gongora-Canul et al., 2020).

Visual estimations of wheat spike blast symptoms were taken seven times, at different days after inoculation (DAI). Wheat spikes of plants of experiment one (4, 6, 9, 12, 14, 16, 19 DAI) and

experiment two (0, 5, 7, 10, 12, 14, 19 DAI) were visually phenotyped, accordingly. Each spike side (four sides total) was assessed visually as the percentage of the area showing spike blast symptoms (C. D. Cruz et al., 2016b; Vales et al., 2018). Simultaneously, an image from each spike side was captured with a DSLR EOS 6D Canon camera (Canon Inc., Tokyo, Japan) using a photography studio setup with umbrellas, lights, and screens that helped create a uniform light and smooth environment (Fig. 3.1c). Each image size was adjusted to 512×256 pixels and used for the DCNN model training.

3.2.4 Disease severity

The criteria for the division of severity categories was based on literature review that indicated that pathologists and breeders considered resistant those cultivars with 20% or less severity (Baldelomar et al., 2015; Cruppe et al., 2020; Cruz et al., 2016a; Fernández-Campos et al., 2020; Vales et al., 2018;). Thus, to define the categories for our DCNN model, the corresponding image and disease severity of the spikes was divided into three categories according to the amount of severity by a pathologist (Rater 1). Non-inoculated spikes were assessed for wheat spike blast severity and served as the negative control. Category 1 included spikes with no symptoms, Category 2 included spikes with low levels of disease symptoms, and Category 3 included spikes with intermediate and high levels of disease symptoms (Tables 3.1 and Table 3.2). The final wheat spike blast severity (Y_{max}) was visually estimated at 19 DAI (Table 3.1), when Atlax, a well-known susceptible cultivar (Cruppe et al., 2020; Cruz et al., 2016a) had reached 100 % of severity.

Table 3.2. Severity ranges of wheat spike blast images per category.

	Category 1	Category 2	Category 3
Severity (%)	0	0.1-20	20.1-100

3.2.5 Inter-rater agreement of wheat spike blast severity estimations

An inter-rater analysis was needed to determine the reliability of visual estimations (Bock et al., 2020; Madden et al., 2007). Inter-rater agreement assesses the degree of agreement between two or more raters who obtain independent ratings about the characteristics of a set of subjects.

Subjects of interest include people, things, or events that are rated (Everitt, 2002). The estimated and measured disease severity values were analyzed for inter-rater agreement in two scenarios, one with a scale of 0-100 % disease severity (continuous data), and the other with the images divided in three categories of disease severity (ordinal data). To determine the degree of agreement between disease estimation by humans and estimations based on measurements made by ImageJ, we computed the Lin's Concordance Coefficient, Fleiss kappa, and weighted kappa statistics.

The Lin's concordance coefficient (ρ_c or CCC) is used to estimate the accuracy₁ between two raters using continuous data. From the analysis, we obtained the estimation of accuracy₁, precision₁, and bias of the disease estimations and disease measurements between two raters (Bock et al., 2010; Lin, L. I.-K., 1989; Madden et al., 2007). For accuracy₁ (ρ_c) and precision₁ (r), values range from 0 to 1; values close to 1 indicate high accuracy₁ and precision₁. Bias (C_b) ranges from 0 to 1, and values close to 1 indicate less bias; however, in this study, bias was represented as $1-(C_b)$ (Nita et al., 2003). Lin's concordance analysis was performed by using PROG REG ALL procedure on SAS v.9.4 (Cary, NC), based on the macro developed by Lawrence Lin and verified by Min Yang (Lin, L. et al., 2002).

To determine the degree of association between estimation of categorical information provided by the two raters (inter-rater agreement), the weighted kappa statistic was computed (Chmura, 1992; Graham and Jackson, 1993; Nelson and Edwards, 2015). The weighted kappa coefficient ranges from 0 to 1. A value from 0.5 to 1 indicates that the agreement is better than what would be expected by chance (Mitani et al., 2017; Tang et al., 2015).

The Fleiss kappa coefficient was used to compare the agreement of categorical information among more than two raters, (i.e. disease severity estimations of Rater 1, Rater 2 and ImageJ) (Fleiss et al., 2003). The value of the Fleiss kappa coefficient ranges from 0 to 1. Values from 0.5 to 1 indicate that the agreement is better than what is expected by chance (Gamer and Maintainer, 2019; Nelson and Edwards, 2015). The Fleiss kappa statistics and weighted kappa were computed with the *irr* package of the R software (Team, 2017).

The power analysis Wilcoxon signed-rank test was selected to determine the sample size for the inter-rater agreement studies of the two training datasets. The test consisted of an evaluation of 31 and 29 images for training Dataset 1 and training Dataset 2, respectively. Two raters assessed the wheat spike blast severity from the corresponding images, and results were compared with the measurement of disease severity from ImageJ. The gold standard of the model was Rater 1 (a

pathologist rater with experience on wheat blast, rice blast, and other diseases), who estimated disease severity from all images used for the training and testing datasets. Rater 2 was an experienced researcher with more than four years working with the wheat blast disease. Raters estimated the disease severity by observing the disease area covered in the spike and assigned a corresponding severity from 0-100%. Subsequently, each image was assigned to a given category (Table 3.2) for ordinal analysis. Spike disease area was manually measured using an (Red Green Blue) RGB color threshold segmentation with Fiji ImageJ v.1.52a (Schindelin et al., 2012). First, we obtained the measurement of the total spike area. Next, we measured the diseased area. Finally, the percent diseased severity (DS) of the individual spike was calculated (Eq. 1), where $A_{Diseased}$ is the proportion of the area of spike that is diseased divided by the total area of the spike A_{Total} .

$$\text{Equation 1.} \quad DS = \frac{A_{Diseased}}{A_{Total}} \times 100$$

3.2.6 Data

Wheat was inoculated at the Feekes 10.5 growth stage of the host plant. Every two days after the inoculation, spike images were collected, allowing us to capture the development of symptoms and corresponding spike blast severity levels. Indirectly, we recorded progressive physiological changes in spikes, from milk and dough stages to maturity (when the spike loses its green color) (Large, 1954). The collected images were divided into three categories, where each category was defined according to a range of disease severity (Table 3.2). Images of healthy spikes, and spikes with moderate and high wheat spike blast severity are shown in Figure 3.2. We trained the proposed DCNN model using two datasets. Dataset 1, which included maturing and non-matured wheat spikes; and Dataset 2, which included only non-matured spikes. Dataset 2 was used because the spike can turn white or yellow as it matures and can mimic spikes with wheat spike blast symptoms, which can lead to confusion when training the model. Each dataset was randomly separated, with 80% of images used as training set, and the remaining 20% as a testing set. Tables 3.3 and 3.4 list the original distribution of the number of images in Dataset 1 and Dataset 2, respectively. However, the number of images in each category was extremely imbalanced, and using them indiscriminately could have resulted in a biased model. Fortunately, there are several viable methods to cope with the disproportionate training data in each category. Data augmentation

was used in this study to balance the number of images in each category. Thus, for Dataset 1, training data was triplicated in Category 2, and quadrupled in Category 3 (Table 3.3). For Dataset 2, training data was quadrupled in Category 2, and quintupled in Category 3 (Table 3.4).

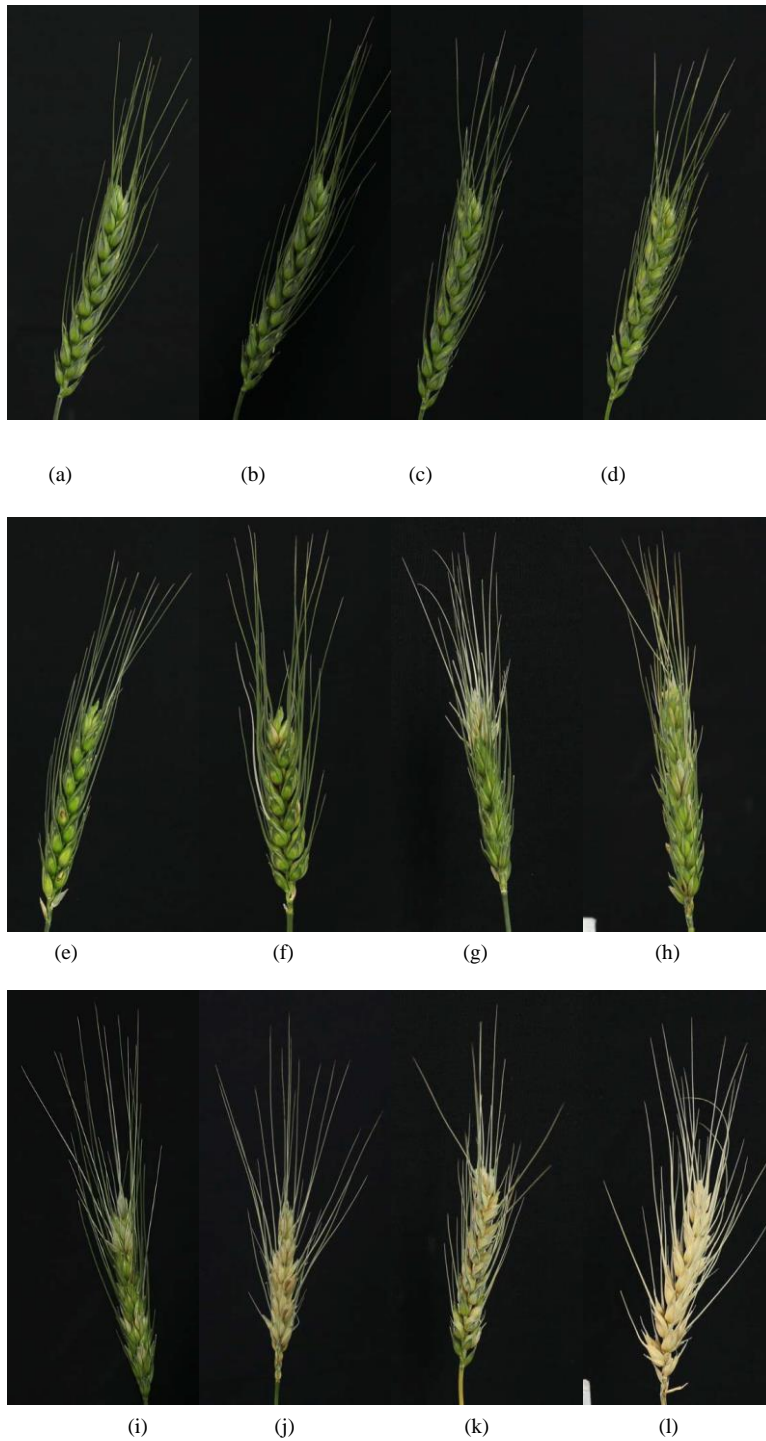


Figure 3.2. Examples of images per category: (a-d) healthy wheat spikes no disease (0% severity, Category 1); (e-h) spikes with moderate severity (0.1-20 %, Category 2); and (i-l) spikes with high severity (20.1-100 %, Category 3).

Table 3.3. Training and testing data distribution and number of images in Dataset 1 (maturing and non-matured spikes)

	Category 1	Category 2	Category 3
Training	1,595	640	402
Training*	1,595	1,920	1,608
Testing	381	178	110

*Augmented training data

Table 3.4. Training and testing data distribution and number of images in Dataset 2 (non-matured spikes only)

	Category 1	Category 2	Category 3
Training	1,430	386	307
Training*	1,430	1,544	1,535
Testing	327	120	90

*Augmented training data

3.2.7 Deep learning model

In recent years, the feasibility of using artificial intelligence, in particular deep learning, is acknowledged by researchers for a variety of applications (Atha and Jahanshahi, 2018; Chen and Jahanshahi, 2018; Kumar et al., 2018; Wu and Jahanshahi, 2019).

Deep learning is a branch in machine learning, which enables computers to automatically extract features from a huge amount of data and learn to classify data. In this study, wheat spike blast symptoms were automatically detected, and classified in three severity categories using a pre-trained DCNN model, which can be more efficient than classifying images visually. To obtain a general and reliable DCNN model, the network needed to be trained using a large labeled training dataset). The wheat blast training dataset was not large enough, and over-fitting could have

occurred. To address this issue, transfer learning was used as a practical solution where a network was trained using a typically different large dataset such as ImageNet. A major advantage of using transfer learning is that it can adapt the parameters trained from an abundant number of images. Transfer learning starts with a pre-trained model, e.g., VGG16 model, and replaces the fully-connected (FC) layers of the model with new FC layers. A network trained on ImageNet dataset was used to initialize the network parameters, and the whole network was fine-tuned since the nature of our dataset was very different from the ImageNet dataset. An FC layer that consists of three nodes, representing three categories, were appended to the end of the network. ResNet101, a DCNN model with 152 layers trained on ImageNet data (He et al., 2016), was selected as the pre-trained model. Furthermore, the loss function, which was used to optimize the parameter in a neural network, was transformed into a weighted loss function (Equation 2) by assigning individual weights to different categories due to the unbalance dataset (number of images in each category was different) in this study. Equation 2 defines the cross-entropy loss function in the DCNN model where $\omega_{category}$ is the assigned weight to each of the category, the first term in equation 2 is a negative log-likelihood loss, and the second term in the is log-softmax. We tested four cases of study with individual weight set to the loss functions assigned to different categories. Here, “cases” refer to specific combinations of weight loss functions for each of the three disease severity categories (Table 3.5). Case 1 was the non-weight set, with all categories sharing the same class weight. Case 2 used [1, 10, 1] class weights in loss function, meaning that the highest weight was for Category 2, which includes plants at early disease stages and low levels of disease symptoms. Case 3 used [2, 5, 1] class weights in loss function, meaning that the higher weight was assigned to Categories 1 (no symptoms) and 2 (early stages and low levels of disease symptoms). Case 4 had class weights [2, 1, 1] in loss function, assigning a higher weight to category 1 (no symptoms) (Table 3.5).

$$\begin{aligned}
 \text{Equation 2. } \quad \text{loss}(x, \text{category}) &= -\omega_{\text{category}} * \log \frac{e^{x_{\text{category}}}}{\sum_{j=1}^N e^{x_j}} \\
 &= -\omega_{\text{category}} \left(-x_{\text{category}} + \log \left(\sum_j \exp(x_j) \right) \right)
 \end{aligned}$$

The network was trained for 15 epochs using stochastic gradient descent (SGD) (Bottou, 2010) optimizer, a learning rate of 0.0001 was used, and the batch size was 16. Additionally, 5-folds cross-validation was applied to the training process. The training took place on a Linux server with Ubuntu 14.04. The server included two Intel Xeon E5-2620 v4 CPUs, 256-GB DDR4 memories, and four NVIDIA Titan X Pascal GPUs. Pytorch (Paszke et al., 2017) was used to implement the DCNN.

Table 3.5. Two datasets trained the four cases of study with different loss functions in three categories. [Category 1: 0%, Category 2: 0.1-20%, Category 3: 20.1-100% severity]

Values of weighted loss function per category [1, 2, 3]		
Model	Dataset 1 (Maturing and non-matured spikes)	Dataset 2 (Non-matured spikes)
Case 1	[1,1,1]	[1,1,1]
Case 2	[1,10,1]	[1,10,1]
Case 3	[2,5,1]	[2,5,1]
Case 4	[2,1,1]	[2,1,1]

3.2.8 Model performance evaluation

The performance of the DCNN model was evaluated via the classified results of the testing dataset. We used a 3×3 confusion matrix to describe the prediction result of the model. Each row of the confusion matrix represented the ground truth of the data, and each matrix column corresponded to a predicted category by the DCNN model. Thus, the diagonal elements of the matrix, called true positive (TP), were the number of wheat images correctly classified into the ground truth. The false positive (FP) for each Category was the sum of the all errors in that column. For example, the FP of Category 1 was the number of Category 2 and 3 severities that were incorrectly classified as Category 1. Based on the confusion matrix, additional evaluation metrics were calculated.

Accuracy₂ was defined as the total number of the TP among three categories divided by the total number of the predictions. Precision₂ was defined as the total number of the TP instances

divided by the total number of predicted positive examples, which was the summation of TP and FP instance in binary classification task (Equation 3). Similarly, the precision₂ of the multi-classes task illustrates the number of instances that were correctly predicted given all the predicted labels for a given category. Recall was defined as TP instance divided by all the positive samples (TP and FN) (Equation 4). F₁ score, a single metric which encompass both precision₂ and recall (Equation 5). Accuracy₂, precision₂, recall, and F₁ score metrics ranged from 0 to 1, where higher values indicate high predictive ability of the model.

$$\text{Equation 3. } Precision_2 = \frac{TP}{TP+FP}$$

$$\text{Equation 4. } Recall = \frac{TP}{TP+FN}$$

$$\text{Equation 5. } F_1score = 2 \times \frac{precision \times recall}{precision + recall}$$

3.3 Results

3.3.1 Cultivar response to wheat spike blast under controlled conditions

All cultivars received a single inoculation with MoT under controlled environmental conditions. Cultivar Atlax exhibited the highest disease severity of all the cultivars and had a high level of susceptibility to wheat spike blast. San Pablo exhibited a moderate susceptibility, while BR-18, Motacú, Urubó and AN-120 exhibited resistance under our controlled environmental conditions (Table 3.2).

3.3.2 Inter-rater agreement analysis

The Lin's concordance correlation analysis showed a high accuracy₁ ($\rho_c = 0.89-0.91$), high precision₁ ($r = 0.91-0.94$), and less bias ($C_b = 0.003-0.0499$) in Dataset 2 than in Dataset 1 ($\rho_c = 0.74-0.85$, precision₁ $r = 0.80-0.90$, and bias $C_b = 0.02-0.09$) (Table 3.6). In Dataset 1, the highest accuracy₁ was between Rater 1 and Rater 2 ($\rho_c = 0.85$) followed by Rater 1 and Image J ($\rho_c = 0.81$). In Dataset 2, the highest accuracy₁ value was between Rater 1 and Image J ($\rho_c = 0.92$), followed by Rater 2 and Image J ($\rho_c = 0.91$). In both datasets, strong accuracy₁, high precision₁, and low bias

involved the ground truth (Rater 1), providing evidence that ratings of disease based on continuous data were done correctly for further classification of the images into categories for model training.

Table 3.6. Values of accuracy₁ (ρ_c), precision₁ (r), and bias (Cb) for agreement between raters' visual estimations and disease measurements of ImageJ in both datasets of wheat spike blast

	Raters	ρ_c	Precision ₁ (r)	Bias (Cb)
	Rater 1 vs ImageJ	0.811	0.896**	0.0943
Dataset 1	Rater 2 vs ImageJ	0.744	0.803**	0.0735
	Rater 1 vs Rater 2	0.846	0.867**	0.0237
	Rater 1 vs ImageJ	0.915	0.942**	0.0292
Dataset 2	Rater 2 vs ImageJ	0.895	0.942**	0.0499
	Rater 1 vs Rater 2	0.912	0.914**	0.0031

** $p < 0.01$

The weighted kappa statistics (κ), used to quantify inter rater-agreement, were higher in Dataset 1 than in Dataset 2, with $\kappa = 0.72-0.88$ ($p < 0.01$) and $\kappa = 0.78-0.85$ ($p < 0.01$), respectively (Table 3.7). In Dataset 1, the highest agreement occurred between Rater 1 and ImageJ ($\kappa = 0.88$), and in Dataset 2 was between Rater 1 and Rater 2 ($\kappa = 0.85$). In both datasets, substantial agreement involved the ground truth (Rater 1), providing evidence that ratings were done correctly for further classification of the images into categories for model training.

Table 3.7. Values of weighted Kappa (κ) analysis for inter-rater agreement between raters and ImageJ in two datasets of wheat spike blast under controlled environment

Categories	Dataset 1		Dataset 2	
	κ	z	κ	Z
Rater 1 vs ImageJ	0.882**	4.93	0.822**	4.45
Rater 2 vs ImageJ	0.727**	4.13	0.776**	4.32
Rater 1 vs Rater 2	0.747**	4.32	0.849**	4.65

** $p < 0.01$

The Fleiss kappa coefficient ($F\kappa$), which compared the association of ordinal categorical information of two or more raters, showed a $F\kappa = 0.77$ for Dataset 1 and 0.69 for Dataset 2, indicating substantial agreement among the three raters in both datasets ($p < 0.001$). However, Dataset 1 possessed a higher Fleiss kappa coefficient index than Dataset 2 (Table. 3.8), both presented substantial agreement between the rates and Image J. Yet, the evidence supported the fact that the three raters correctly estimated the amount of the disease from the same image.

Table 3.8. Values of Fleiss Kappa ($F\kappa$) analysis among two raters and ImageJ agreement in two datasets of wheat spike blast under a controlled environment

	κ	n	z	p>F
Dataset 1	0.771	31	9.26	<0.0001
Dataset 2	0.697	29	8.1	<0.0001

3.3.3 Deep convolutional neural networks model performance.

To train the proposed DCNN model, we used two different datasets. As mentioned in Section 3.2.6, Dataset 1 included matured and non-matured wheat spikes. On the other hand, Dataset 2 included only non-matured spikes. Four cases were applying different weight set of loss functions in both Datasets. Case 1 was the non-weight set, meaning that all categories shared the same class weight. Case 2 used [1, 10, 1] class weights in loss function, Case 3 used [2, 5, 1] class weights in

loss function, and Case 4 had class weights [2, 1, 1] in loss function. The performance of the DCNN model was evaluated via the classified result of testing data.

The testing accuracy₂ of the model trained with Dataset 1 was 90.1% in Case 1, 90.4% in Case 2, 90% in Case 3, and 87.7% in Case 4. The testing accuracy₂ of Dataset 2 was 98.4% in Case 1, 93.9% in Case 2, 95.0% in Case 3, and 94.2% in Case 4. Dataset 2 presented higher accuracy₂ values compared to Dataset 1, suggesting that the model was accurate. However, it was not sufficient to claim the model was reliable based on accuracy₂ (model performance metric) alone since the dataset in this study was unbalanced. In addition to accuracy₂, other metrics can help evaluate the performance of the DCNN model such as precision₂, recall, and F₁ score.

Precision₂ indicates the ability to correctly classify an instance in all predicted positive instances. We wanted to focus on DCNN model's performance in Category 2 as this was the category that breeders and pathologists will concentrate on for breeding purposes. Dataset 1 Case 2 showed the lowest precision (75.4%) among all cases value (Table 3.9). Moreover, the confusion matrix of Dataset 1 Case 2 showed that the model misclassified 38 images of Category 1 (no symptoms) as Category 2 (early disease stages and low levels of disease symptoms), which was the highest number of wrongly classified images among all the cases (Fig. 3.3b). This suggested that the class weight of Category 2 might be too high since it misclassified images that belonged to other categories as Category 2. Hence, the class weight combination was modified by lowering the weight in Category 2 and increasing the weight in Category 1 as to not overemphasize the impact from Category 2. Precision₂ of Category 2 significantly increased from 75.4% in Case 2 to 84.1% in Case 3, and to 85% in Case 4. (Table 3.9). In Case 2, precision₂ of Category 2 significantly increased, from 75.4% in Dataset 1, to 90.2% in Dataset 2 (Table 3.9). Precision₂ of Category 2 significantly increased from 90.2% in Case 2 to 92.7% in Case 3, and to 94.1% in Case 4 (Table 3.9).

Another metric for evaluating DCNN model was recall, which indicates the ability to correctly recognize a category. In Dataset 1 and 2, the recall of Category 2 was the lowest, illustrating the model's challenge to classify images of Category 2 (early disease stages and low levels of disease symptoms) (Table 3.9). The highest recall of Dataset 1 Category 2, was 86.0% in Case 2, and the lowest was 74.2% in Case 1 (Table 3.9). This was expected given that Case 2 had higher weight in loss function of Category 2 compared to Case 1 (non-weighted loss function). In Case 2, Dataset 1, the recall values were similar among the three categories (Table 3.9). In Dataset

2 Category 2, the lowest recall was 75.0% in Case 1, and the highest recall was 84.2% in Case 2 and 3 (Table 3.9). The model in these two cases had the highest weight in loss function of Category 2 (early disease stages and low levels of disease symptoms).

F₁ score is a common indicator of the DCNN model’s overall performance. In Dataset 1 and 2, the F₁ score of Category 2 was the lowest, reaffirming the difficulty of classifying images of Category 2 by the model (Table 3.9). The lowest F₁ score of Dataset 1 Category 2, was 79.3% in Case 1, while the highest was 82% in both Case 3 and Case 4 (Table 3.9). In Dataset 2 Category 2, the lowest F₁ score was 82.6% in the Case 1, and the highest F₁ score was 88.2% in Case 3 followed by Case 2 with 87.1% (Table 3.9).

Table 3.9. Precision, recall and F₁ score of the test data for different model in both datasets.

		Dataset 1			Dataset 2		
Model	Performance Index	Category 1	Category 2	Category 3	Category 1	Category 2	Category 3
Case 1	Precision	0.891	0.852	0.955	0.923	0.918	0.967
	Recall	0.945	0.742	0.955	0.985	0.750	0.967
	F-1	0.917	0.793	0.955	0.953	0.826	0.967
Case 2	Precision	0.926	0.754	0.950	0.952	0.902	0.936
	Recall	0.890	0.860	0.864	0.963	0.842	0.978
	F-1	0.908	0.803	0.905	0.957	0.871	0.957
Case 3	Precision	0.915	0.841	0.938	0.953	0.927	0.967
	Recall	0.929	0.803	0.955	0.985	0.842	0.967
	F-1	0.922	0.822	0.946	0.968	0.882	0.967
Case 4	Precision	0.915	0.850	0.946	0.942	0.941	0.946
	Recall	0.937	0.798	0.964	0.991	0.792	0.967
	F-1	0.926	0.823	0.955	0.966	0.860	0.956

A comparison of outcomes revealed that Category 2 was the most difficult category to classify correctly (Figure 3.3). This difficulty was attributed to the disease symptoms being barely visible at the early stage of infection, and some wheat spikes in Category 1 were maturing, and their color were similar to that of MoT infected spikes. We observed that the highest number of images exactly classified as Category 2 was obtained with the Case 2 Dataset 1 (Figure 3.3b). These results suggested that Case 2 was the most appropriate to classify wheat spike blast images in Dataset 1 because it was capable of detecting the infection at an early stage. Even though Case 2 had a slightly lower precision, we consider this usual trade-off between precision₂ and recall for disease classification purposes. The recall, precision₂, and F₁ score increased after the images of maturing spikes were omitted when training the model with Dataset 2 (Figure 3.4). The Cases 2 and 3 of Dataset 2 presented the highest number of images exactly classified as Category 2 (Figure 3.4b,c). Cases 2 and 3 were the most appropriate to detect the wheat spike blast in Dataset 2 because the model was capable of detecting the infection in early stages. Additionally, in all Cases, the model was more stable predicting Category 3, which is relevant because it covers disease severity from 20.1 to 100%, potentially aiding breeders and pathologists to discern higher levels of susceptibility among cultivars. Although the DCNN model misclassified some images of Category 2, it still provided a robust approach to classify the severity of the disease. Moreover, the computational time for estimation of disease severity of a single image was 0.02 seconds.

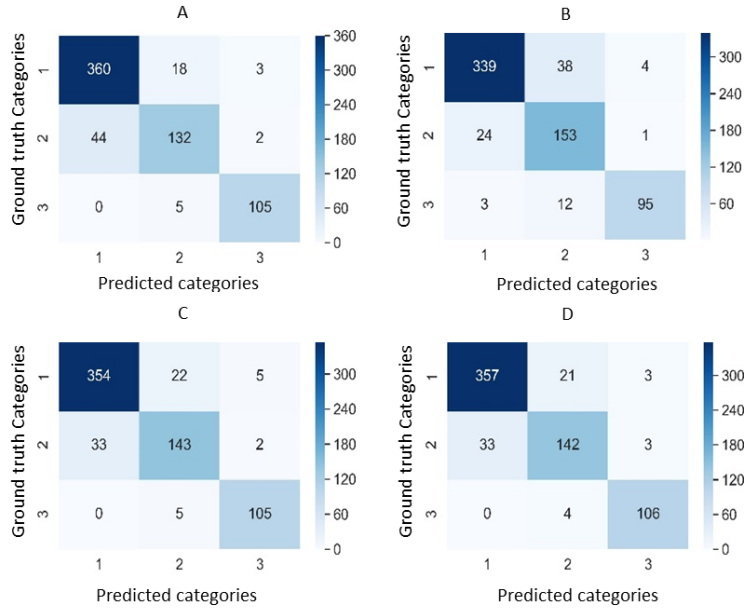


Figure 3.3. Confusion matrix of the images of Dataset 1 (maturing and non-matured spikes): (A) Case 1, (B) Case 2, (C) Case 3 and (D) Case 4

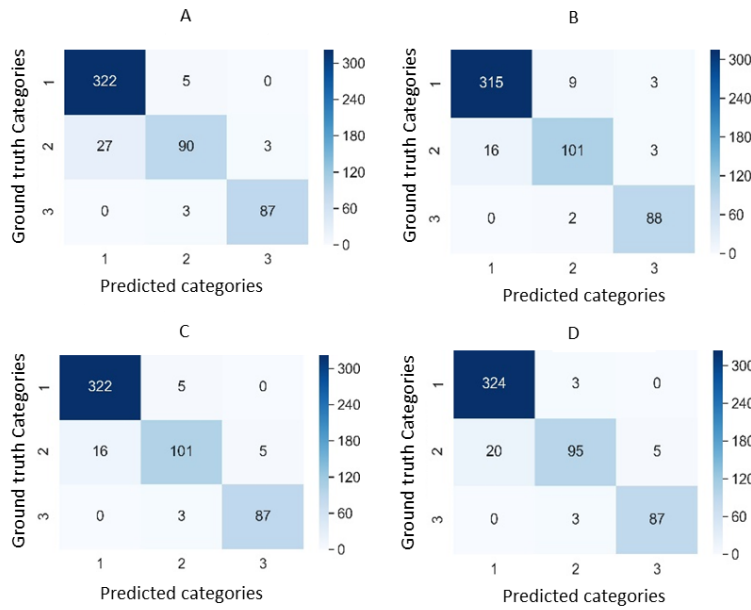


Figure 3.4. Confusion matrix of the images of Dataset 1 (non-matured spikes only): (A) Case 1, (B) Case 2, (C) Case 3 and (D) Case 4

3.4 Discussion

This is the first study presenting a deep convolutional neural networks model to detect, quantify, and classify wheat spike blast symptoms in three severity categories under controlled environments. Wheat spike blast symptoms developed on all tested cultivars, with reactions to MoT infection consistent with previous reports, except for BR-18 and San Pablo that showed resistance and moderate susceptibility, respectively (Baldelomar et al., 2015, Cruppe et al., 2020; Gongora-Canul et al., 2020; Cruz et al., 2016a). Images of spikes with and without wheat spike blast symptoms were useful for non-destructive disease estimation by humans and disease measurement by image analysis. There was a consistent agreement of disease severity estimations between and among raters, using continuous and discrete data. In general, there was a higher agreement when using percent disease severity (continuous data) compared to categorical data. A DCNN model trained with percent disease severity data is challenging because it requires multiple images showing symptoms of each disease severity percentage (i.e. 300 images of 50% severity, 300 images 68% severity). Multiple images of each disease severity percentage were limited in this study, thus categorical data was used to train the DCNN model. Nevertheless, agreement analysis of categorical data showed substantial agreement in disease estimations and measurements between raters and Image J, respectively. The ground truth (Rater 1) was consistently in agreement with other raters. The results showed that the DCNN model correctly classified wheat spike blast images in the corresponding severity categories with an average accuracy₂, precision₂, recall and F₁ score up to 0.98, 0.97, 0.98, 0.97, respectively. Consequently, the proposed approach is promising for wheat spike blast severity evaluation under controlled environment conditions, supported by a substantial agreement between disease estimations of the ground truth, an expert in wheat blast and the disease measurement of Image J. Wheat breeders could benefit from the proposed model classification. They can do a pre-selection of wheat cultivars under a controlled environment, taking images of spikes and classifying them automatically with the wheat spike blast DCNN model. Next, the breeders can focus on the cultivars that fall into Categories 1 and 2, which in general terms, are considered resistant or moderately resistant, which may reduce the high number of cultivars tested under field conditions. More research in this area is needed, mainly under field conditions where the environment can affect the output of the model. Nevertheless, the promising model and results of this study establish a foundation of using state-of-the-art computer vision techniques in wheat blast. The wheat spike

blast DCNN model may accelerate cultivar screening and identification of new sources of wheat spike blast resistance. Also, the results in this study show an opportunity to apply a similar approach in other pathogens.

3.5 Conclusion

Wheat blast is spreading worldwide, and a few resistant cultivars are available. It is crucial to identify more resistant sources, consequently more cultivars disease estimations are needed, an alternative can be testing more cultivars under controlled environments using a wheat spike blast deep convolutional neural networks model. Moreover, a wheat spike blast dataset was obtained with 3,306 images labeled with each respective disease severity estimation. The labeled disease severity estimation attached at each image of the training datasets used for the deep convolutional neural networks model demonstrated substantial agreement with the disease estimations of an expert in wheat blast and disease measurement of ImageJ. This is the first study presenting a deep convolutional neural network model trained to detect and classify wheat spike blast symptoms in three severity categories, which can aid in pre-screening of wheat blast cultivar resistance under controlled conditions.

The deep convolutional neural networks model was trained to classify only three categories and is limited to images of wheat spike blast under controlled conditions. In the future, variability in disease estimations can be reduced if we standardize protocols (Cruz et al., 2016a), especially with state-of-the-art technology as deep learning (Yang et al., 2020). The next step in this research is to deploy the model in a web app where breeders and pathologists can submit their images, and the model will automatically classify them by categories. More images of wheat spike blast infected with different isolates will add symptom variability and make the model more robust to improve the proposed model. The model can eventually be retrained with multiple images of each disease severity percentage, allowing flexibility to predict wheat spike blast severity beyond the three categories.

3.6 References

- Atha, D. J., & Jahanshahi, M. R. 2018. Evaluation of deep learning approaches based on convolutional neural networks for corrosion detection. *Structural Health Monitoring*. 17(5), 1110-1128.
- Baldelomar, D., Cardenas, S., & Quispe, K. 2015. Caracterización de genotipos de trigo (*Triticum aestivum*) con resistencia a piricularia durante el verano 2014/2015 en Quirusillas, Santa Cruz, Bolivia. *INIAF* (online) vol.1, n.6, pp. 17-21. ISSN 2308-250X.
- Barbedo, J. G. A. 2016. A review on the main challenges in automatic plant disease identification based on visible range images. *Biosystems engineering* .144, 52–60.
- Bock, C. H., Barbedo, J. G. A., Del Ponte, E. M., Bohnenkamp, D., & Mahlein, A.-K. 2020. From visual estimates to fully automated sensor-based measurements of plant disease severity: status and challenges for improving accuracy. *Phytopathology Research*. 2(1), 1–30.
- Bock, C. H., Poole, G. H., Parker, P. E., & Gottwald, T. R. 2010. Plant disease severity estimated visually, by digital photography and image analysis, and by hyperspectral imaging. *Critical Reviews in Plant Sciences*. 29(2), 59-107.
- Bottou, L. 2010. Large-scale machine learning with stochastic gradient descent. In Y. Lechevallier and G. Saporta (Eds.), *Proceedings of compstat*. 177–186. Heidelberg: Physica-Verlag HD.
- Brahimi, M., Arsenovic, M., Laraba, S., Sladojevic, S., Boukhalifa, K., & Moussaoui, A. 2018. Deep learning for plant diseases: Detection and saliency map visualisation. *Human and machine learning*. 93–117.
- Camargo, A., & Smith, J. S. 2009. Image pattern classification for the identification of disease causing agents in plants. *Computers and Electronics in Agriculture*. 66(2), 121–125.
- Cardoso, R. E. M., C. A., and Moreira, E. N. (2008). Development of a warning system for wheat blast caused by *Pyricularia grisea*. *Summa Phytopathologica*. 34, 216–221.
- Ceresini, P., Castroagudín, V. L., Rodrigues, A., F., Rios, J., Aucique-Pérez, C., Moreira, S. I., & McDonald, B. 2019. Wheat blast: from its origins in South America to its emergence as a global threat. *Phytopathology*. 104:95-107.
- Chen, F., & Jahanshahi, M. R. 2018. Deep learning-based crack detection using convolutional neural network and naïve bayes data fusion. *IEEE Transactions on Industrial Electronics*. 65(5), 4392-4400.
- Chmura, H. 1992. Measurement of reliability for categorical data in medical research. *Statistical Methods in Medical Research*. 1, 183–199.
- Cruppe, G., Silva, P., da Silva, C.L., Peterson, G., Pedley, K.F., Cruz, C.D., Asif, M., Lollato, R.P., Fritz, A.K. & Valent, B. 2020. Genome wide association reveals limited benefits of pyramiding

the 1B and 1D loci with the 2N^VS translocation for wheat blast control. *Crop Science*. <https://doi.org/10.1002/csc2.20397>.

Cruppe, G., Cruz, C., Peterson, G., Pedley, K., Mohammad, A., Fritz, A., & Valent, B. 2019. Novel sources of wheat head blast resistance in modern breeding lines and wheat wild relatives. *Plant Disease*. 104, 35–43.

Cruz, C.D. & Valent, B. 2017. Wheat blast disease: danger on the move. *Tropical Plant Pathology*. 42, 210–222.

Cruz, C. D., Bockus, W., Stack, J., Valent, B., Maciel, J. N., & Peterson, G. L. 2016b. A standardized inoculation protocol to test wheat cultivars for reaction to head blast caused by *Magnaporthe oryzae* (triticum pathotype). *Plant Health Progress*. 17(3), 186–187.

Cruz, C. D., Peterson, G. L., Bockus, W. W., Kankanala, P., Dubcovsky, J., Jordan, K. W., & Valent, B. 2016a. The 2N^VS translocation from *aegilops ventricosa* confers resistance to the triticum pathotype of *Magnaporthe oryzae*. *Crop Science*. 56, 990–1000.

Cruz, C. D., Kiyuna, J., Bockus, W., Todd, T. C., Stack, J. P., & Valent, B. 2015. *Magnaporthe oryzae* conidia on basal wheat leaves as a potential source of wheat blast inoculum. *Plant Pathology*. 64, 1491-1498.

Everitt, B. 2002. *The Cambridge dictionary of statistics*. Cambridge University Press.

Fernández-Campos, M., Góngora-Canul, C., Das, S., Kabir, M., Valent, B., & Cruz, C. 2020. Epidemiological criteria to support breeding tactics against the emerging, high-consequence wheat blast disease. *Plant Disease*. 104 (8), 1–38.

Fleiss, J. L., Levin, B., & Paik, M. C. 2003. *Statistical methods for rates and proportions*. John Wiley and Sons, Inc. Gamer, M., and Maintainer. (2019). Package 'irr' title various coefficients of interrater reliability and agreement (Tech. Rep.).

Ghosal, S., Blystone, D., Singh, A. K., Ganapathysubramanian, B., Singh, A., & Sarkar, S. 2018. An explainable deep machine vision framework for plant stress phenotyping. *Proceedings of the National Academy of Sciences of the United States of America*. 115(18), 4613–4618.

Gongora-Canul, C., Salgado, J., Singh, D., Cruz, A., Cotrozzi, L., Couture, J. J., & Cruz, C. D. 2020. Temporal dynamics of wheat blast epidemics and disease measurements using multispectral imagery. *Phytopathology*. 110, 393-405.

Graham, P., & Jackson, R. 1993. The analysis of ordinal agreement data: Beyond weighted kappa. *Journal of Clinical Epidemiology*. 46(9), 1055–1062.

He, K., Zhang, X., Ren, S., and Sun, J. 2016. Deep residual learning for image recognition. In *2016 IEEE conference on computer vision and pattern recognition (cvpr)*, 2016. IEEE. 770–778

- Igarashi, S. 1986. *Brusone no trigo- histórico e distribuição geográfica no Paraná*. In: *Reunião nacional de pesquisa de trigo*, 15 (Tech. Rep.).
- Igarashi, S., Utiamada, C. M., Kazuma, I. L. C., H., A., & Lopes, R. S. 1986. Pyricularia em trigo. I. Ocorrência de *Pyricularia sp.* no estado do Parana. *Fitopatol. Bras.* 11, 351-352.
- Kumar, S., Kashyap, P. L., Mahapatra, S., Jasrotia, P., & Singh, G. P. 2020. New and emerging technologies for detecting *Magnaporthe oryzae* causing blast disease in crop plants. *Crop Protection*, 105473.
- Kumar, S. S., Abraham, D. M., Jahanshahi, M. R., Iseley, T., & Starr, J. 2018. Automated defect classification in sewer closed circuit television inspections using deep convolutional neural networks. *Automation in Construction*. 91, 273 - 283.
- Large, E. C. 1954. Growth stages in cereals illustration of the feeks scale. *Plant Pathology*. 3(4), 128–129.
- Lin, L., Hedayat, A. S., Sinha, B., & Yang, M. 2002. Statistical methods in assessing agreement. *Journal of the American Statistical Association*. 97, 257–270.
- Lin, L. I.-K. 1989. A concordance correlation coefficient to evaluate reproducibility. *Biometrics*, 45, 255.
- Lobet, G. 2017. Image Analysis in Plant Sciences: Publish Then Perish. *Trends in Plant Science*. 22, 559–566.
- Lu, J., Hu, J., Zhao, G., Mei, F., & Zhang, C. 2017. An in-field automatic wheat disease diagnosis system. *Computers and Electronics in Agriculture*. 142, 369–379.
- Madden, L. V., Hughes, G., and van den Bosch, F. 2007. The study of plant disease epidemics. *The American Phytopathological Society*.
- Mahlein, A.-K, 2015. Precision agriculture and plant phenotyping are information-and technology-based domains with specific demands and challenges for. *Plant disease*. 100(2), 241-251.
- Mitani, A. A., Freer, P. E., & Nelson, K. P. 2017. Summary measures of agreement and association between many raters' ordinal classifications. *Elsevier Inc*. 27
- Mohanty, S. P., Hughes, D. P., & Salathé, M. 2016. Using deep learning for image-based plant disease detection. *Frontiers in Plant Science*. 7, 14-19
- Nelson, K., & Edwards, D. 2015. Measures of agreement between many raters for ordinal classifications. *Statistics in Medicine*. 34(23), 3116–3132.
- Nita, M., Ellis, M. A., & Madden, L. V. 2003. Reliability and accuracy of visual estimation of Phomopsis leaf blight of strawberry. *Phytopathology*. 93, 995–1005.

- Nutter, F. W., Gleason, M., Jenco, J., & Christians, N. 1993. Assessing the accuracy, intra-rater repeatability, and inter-rater reliability of disease assessment systems. *Phytopathology*. 83, 806–812.
- Paszke, A., Gross, S., Chintala, S., Chanan, G., Yang, E., DeVito, Z., & Lerer, A. 2017. Automatic differentiation in PyTorch. In *Nips autodiff workshop*.
- Prestes, A. M., Arendt, P. F., Fernandes, J. M. C., & Scheeren, P. L. 2007. Resistance to *Magnaporthe grisea* among brazilian wheat genotypes. *Springer Netherlands*. 16, 119-123
- Shakoor, N., Lee, S., & Mockler, T. C. 2017. High throughput phenotyping to accelerate crop breeding and monitoring of diseases in the field. *Current Opinion in Plant Biology*. 38, 184–192.
- Schindelin, J., Arganda-Carreras, I., Frise, E., Kaynig, V., Longair, M., Pietzsch, T., & Cardona, A. 2012. Fiji: an open-source platform for biological-image analysis. *Nature Methods*. 9, 676 - 682.
- Singh, A., Ganapathysubramanian, B., Sarkar, S., & Singh, A. 2018. Deep learning for plant stress phenotyping: Trends and future perspectives. *Trends in Plant Science*. 23, 883–898.
- Tang, W., Hu, J., Zhang, H., Wu, P., & He, H. 2015. Kappa coefficient: a popular measure of rater agreement. *Shanghai Archives of Psychiatry*. 27, 62–67.
- Team, R. C. 2017. R: A language and environment for statistical computing (Computer software manual). Vienna, Austria.
- Tembo, B., Mulenga, R. M., Sichilima, S., M’siska, K. K., Mwale, M., Chikoti, P. C., & Braun, H. J. 2020. Detection and characterization of fungus (*Magnaporthe oryzae* pathotype *Triticum*) causing wheat blast disease on rain-fed grown wheat (*Triticum aestivum* L.) in Zambia. *PLOS ONE*, 15(9).
- Urashima, A., Lavorent, N. A., Goulart, A. C. P., & Mehta, Y. R. 2004. Resistance spectra of wheat cultivars and virulence diversity of *Magnaporthe grisea* isolates in brazil. *Fitopatologia Brasileira*. 29, 511-518.
- Vales, M., Anzoátegui, T., Huallpa, B., & Cazon, M. I. 2018. Review on resistance to wheat blast disease (*Magnaporthe oryzae Triticum*) from the breeder point-of-view: use of the experience on resistance to rice blast disease. *Euphytica*. 214(1), 1–19.
- Wu, R.-T., & Jahanshahi, M. R. 2019. Deep convolutional neural network for structural dynamic response estimation and system identification. *Journal of Engineering Mechanics*. 145(1), 04018125.

Yang, W., Feng, H., Zhang, X., Zhang, J., Doonan, J. H., Batchelor, W. D., Xiong, L. and Yan, J. 2020. Crop Phenomics and High-Throughput Phenotyping: Past Decades, Current Challenges, and Future Perspectives. *Molecular Plant*. 13 (2), 187-214.